https://doi.org/10.5194/egusphere-2026-1873
Preprint. Discussion started: 10 April 2026

Biogeochemical regimes control marine aerosol emission of hydrogels in the Southwestern Pacific Ocean

Theresa Barthelmeß[1*], Karine Sellegri[3], Benjamin Pontiller[1], Lindsay Scheidemann[2], Karl Safi[4], Anja Engel[1]

[1]GEOMAR, Helmholtz Centre for Ocean Research Kiel, 24105 Kiel, Germany.
[2]*Formerly at* GEOMAR, Helmholtz Centre for Ocean Research Kiel, 24105 Kiel, Germany.
[3]Université Clermont Auvergne, CNRS, Laboratoire de Météorologie Physique (LaMP), 63000 Clermont-Ferrand, France.
[4]National Institute of Water and Atmospheric Research (NIWA), 6021 Wellington, New Zealand.

Correspondence to: Theresa Barthelmeß (tbarthelmess@geomar.de)

Abstract. Ambient marine aerosols are frequently enriched in biogenic material. It was suggested that a critical fraction may be attributed to colloids and aggregates, which are composed of carbohydrates and proteins. Those hydrogels possess excellent cloud condensation and ice nucleation properties. Yet, most atmospheric measurements fail to detect marine hydrogels in aerosols directly, and the few studies which exist were conducted in the Northern hemisphere. Here, we present a comprehensive data set of carbohydrate and protein-enriched hydrogels in in sea spray aerosols (SSA) generated within representative regimes of the Southwestern Pacific Ocean. We relate the concentration of hydrogels in SSA to the occurrence of their precursors in surface seawater and other biogeochemical variables. The highest concentration ($0.91 \pm 0.72 \times 10^5$ m^{-3}, corresponding to $4.1 \pm 2.1 \times 10^3$ particles ng^{-1} Na^+) and highest relative enrichment ($5.3 \pm 3.9 \times 10^5$) of hydrogels in SSA (size range: 0.5-30 µm) was observed within the subtropical front, which is biologically most active. This was contrasted by subtropical waters, in which SSA concentration and enrichment decreased by one order of magnitude. Interestingly, the carbohydrate-to-protein ratio shifted with size in SSA hydrogels, while no such size-shift existed for marine samples. In comparison to their marine precursors, supermicron hydrogels in SSA were primarily composed of carbohydrates. Our results suggest that hydrogels may complement a considerable fraction of ambient marine aerosols, and significantly contribute to the atmospheric pool of cloud condensation and ice nuclei, in particular above the remote oceans of the Southern hemisphere.

https://doi.org/10.5194/egusphere-2026-1873
Preprint. Discussion started: 10 April 2026

1 Introduction

Organic matter with the signature of carbohydrates is often enriched in freshly emitted sea spray aerosols (SSA) and ambient marine aerosols (Jayarathne et al., 2016; Russell et al., 2010; Wang et al., 2015). It was suggested that hydrogels, assembled from carbohydrates and proteins and released by microscopic ice algae or phytoplankton, dominate the ambient marine aerosol pool above Arctic waters in summer (Orellana et al., 2011). Facchini et al. (2008) reported that submicron biogenic aerosols (<1.0 µm), produced during a phytoplankton bloom above the North Atlantic, likely consisted of aggregates and colloids resembling in their size spectra abundant ambient aerosols (O'Dowd et al., 2004). The emission of carbohydrate- and protein-like hydrogels from oceanic surface waters has been demonstrated over the western North Atlantic (Aller et al., 2017). Recently, it was observed that carbohydrate-like hydrogels were highly enriched in ambient aerosols and cloud water above the subtropical North Atlantic (Pinxteren et al., 2022). Hydrogels have been suggested to serve as cloud condensation nuclei (CCN) and ice nucleating particles (INP) and therewith stimulate cloud formation (Leck & Bigg, 2005; Orellana et al., 2011; Ovadnevaite et al., 2011; Wilson et al., 2015; Hartmann et al., 2025). The ability to initiate cloud formation likely relates to the surface-active structure of hydrogels, which facilitates the arrangement of water molecules while water transfer across the aerosol interface is still permitted (Hasenecz et al., 2019). The incorporation of enzymes (proteins) enhances the stability and enrichment of a polymeric carbohydrate matrix in SSA (Hasenecz et al., 2019). Proteins embedded in lipid monolayers reduce monolayer resistance and therewith increase the hygroscopicity of SSA, further contributing to cloud condensation activity (Luo et al., 2019). Protein aggregates and enzymes are ubiquitously present in the marine realm and SSA, where they represent excellent and persistent ice nuclei (Alsante et al., 2023; Cascajo-Castresana et al., 2020; Malfatti et al., 2019). Upon their introduction in small droplets, heterogeneous freezing is initiated, enabling ice cloud formation already at temperatures as high as -5°C (Alsante et al., 2023; Cascajo-Castresana et al., 2020). It has been argued that rather supermicron (diameter > 1 µm) than submicron marine aerosols act as potent INPs (McCluskey et al., 2017; Mitts et al., 2021). Most recent estimates attribute 44% of marine INPs in the atmosphere to carbohydrate-enriched aerosols (Hartmann et al., 2025).

In the surface ocean, phytoplankton is responsible for roughly half of the global carbon dioxide fixation (Behrenfeld et al., 2005; Moran et al., 2022). The oceanic organic carbon reservoir is as large as the carbon inventory of the atmosphere (~662 Pg C) (Hansell et al., 2009). It was suggested that at least 10% of marine organic carbon fixed by phytoplankton is channeled into the extracellular, particulate phase (>0.5 µm) in the form of hydrogels, reaching an equilibrium of assembly and dispersion (Mari et al., 2017; Verdugo, 2012). Marine hydrogels composed of carbohydrates and proteins include transparent exopolymer particles (TEP) and Coomassie stainable particles (CSP), respectively (Alldredge et al., 1993; Long & Azam, 1996). While TEP occurrence in the marine realm is fairly well explored, comprehensive studies on CSP are still rare (Cisternas-Novoa et al., 2015; Engel et al., 2020). Carbohydrates and proteins are released by phytoplankton and its complex bacterial associates, but the causes of release may differ and span from photosynthetic overflow to grazing and viral lysis (Engel et al., 2020; Thornton, 2014). Detached from cells, TEP are neutrally or even positively buoyant and easily manipulated to ascent or descent

https://doi.org/10.5194/egusphere-2026-1873
Preprint. Discussion started: 10 April 2026

within the water column (Mari et al., 2017). Furthermore, bubble intrusion by wind and wave forcing, enhances CSP and TEP accumulation within the sea surface microlayer (SML) (Robinson et al., 2019; Sun et al., 2018). Bubbles ultimately burst at the surface, ejecting SSA into the atmosphere (Deike, 2021). SSA is produced by two mechanisms: Either, the film cap of a bubble bursts into fragments (Lhuissier & Villermaux, 2012; Poulain & Bourouiba, 2018), or the bubble cavity collapses and ejects jet droplets (Villermaux et al., 2022). Both droplet populations transport organic material (Blanchard, 1989; Crocker et al., 2022; Wang et al., 2017).

Although hydrogels seem to be important components of the biogenic aerosol pool, the majority of atmospheric analyses fail to detect hydrogels directly, and thus data are scarce (Brooks & Thornton, 2018). While SSA may become highly enriched in biogenic material and in relation to biological activity (Burrows et al., 2014; Jayarathne et al., 2016; Long et al., 2014), oceanic conditions promoting hydrogel emission are yet to be explored. Moreover, most campaigns exploring hydrogels in SSA or ambient aerosols were conducted over the North Atlantic and none within the Southern hemisphere, in which remote oceanic waters balance cloud albedo (Blanco et al., 2023) most likely via the emission of marine biogenic aerosols (McCoy et al., 2015; Hartmann et al., 2025). Based on a comparison of four regimes in the Southwestern Pacific Ocean, which were distinct in their biological activity, we here investigate biological factors influencing the occurrence of hydrogels in SSA. A bubble bursting chamber with a plunging-jet system was applied to mimic the natural spectra of SSA (Fuentes et al., 2010; Sellegri, Barthelmeß, et al., 2023). Here, we explore the size-dependent, heterogeneous nature of hydrogels in SSA by discriminating between four size bins as well as carbohydrate and protein-like components. We relate the occurrence and composition of hydrogels in surface seawater (TEP and CSP) to the emission of hydrogels in SSA and outline potential source mechanisms.

2 Methods

2.1 Sampling

Surface samples were collected from board of the RV Tangaroa east of the Southern New Zealand Island in March 2020. Four oceanic regimes were defined based on salinity and nutrient profiles and are described in greater detail elsewhere (Barthelmeß et al., 2025; Saint-Macary et al., 2023; Sellegri, Harvey, et al., 2023). In brief, sub-Antarctic (SAW) and subtropical waters (STW) converge along the Chatham Rise creating the subtropical front (STF), which is characterized by high biological activity due to replenished macro- and micronutrients. STW mixed with waters from the Cook Strait are referred to as MIX (Fig. 1, Table A1). SSA were generated by a plunging-jet system (chamber volume 10 L) as schematically presented in Sellegri, Barthelmeß, et al., (2023) and originally introduced by Fuentes et al., (2010). The walls and lid of the chamber were built of glass and stainless steel, respectively. The bubble chamber was continuously supplied with seawater from the underway system (depth ~6 m), and filled up to 3.6 L, which is equivalent to a water depth of 10 cm. The residence time of the water in the chamber was ~4 min. SSA were produced by splashing water through jets onto the water surface of the chamber. The water was injected at a rate of 1.2 L min^{-1} (Sellegri, Barthelmeß, et al., 2023). Aerosol size distribution produced by the plunging-jet

https://doi.org/10.5194/egusphere-2026-1873
Preprint. Discussion started: 10 April 2026

system corresponds best to the natural spectra of SSA droplets (Fuentes et al., 2010) and also includes large aerosols (coarse mode) (Sellegri, Barthelmeß, et al., 2023), which are potentially derived from jet droplets (Wang et al., 2017). The air outflow was sampled for aerosols, after being dried by passing it over a silica gel diffusive drier (<40% relative humidity). An overview including the duration of aerosol collection and filtered air volume is provided in Table A2.

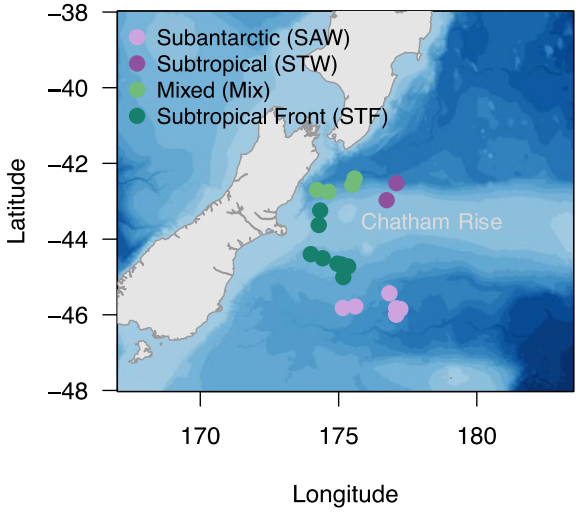

Figure 1 Sampling region in the Southwestern Pacific Ocean along the Chatham rise. Regimes are delineated according to salinity and nutrient profiles.

2.2 Analysis of hydrogels in surface seawater (SSW) and sea spray aerosols (SSA)

SSW samples were collected from the ship's underway supply (n=13) or from a small working boat (n=7). Samples were collected at local times in the morning (08:00 AM) and afternoon (04:00 PM), and in concert with further parameters such as total Chlorophyll *a* (Chl a), *Synechococcus* spp., pico-, and nano-phytoplankton cell abundance, heterotrophic bacteria counts, particulate and dissolved amino acids (PAA/DAA), particulate and dissolved combined carbohydrates (PCCHO/DCCHO), total organic carbon (TOC), and total organic nitrogen (TON) (methods described in more detail in Sellegri et al., 2023, and Barthelmeß et al., 2025). For CSP and TEP, an adequate volumes (CSP: 45 ± 8 mL, range: 30-70 mL; TEP: 61 ± 16 mL, range: 30-80) of surface seawater (SSW) was filtered onto 0.45 µm pore size polycarbonate filters (25 mm, Nucleopore, Whatman) and stained with Coomassie Brilliant Blue G and Alcian Blue following the protocol of Engel (2009). After air-drying, CSP and TEP duplicates were stored on microscopic slides using microscopy oil (refractive index 1.584, Cargille) and a coverslip, then frozen at -20 °C until the analysis. As blanks, 10 mL of MilliQ water was filtered. In total, 20 surface samples and 8 blanks were prepared. Averaged absolute blank values were subtracted before the data analysis. Relative standard deviation (rSD) between CSP duplicates (n=18) differed between size bins but was well below 20% with respect to particle abundance (rSD: 9 ± 9%) and area (12 ± 8%) for 90% and 85% of CSP samples, respectively. Relative standard deviation between TEP duplicates (n=20) was in general smaller than 20% with respect to particle abundance (rSD: 13 ± 8%) and area (10 ± 7%) for 80% and 95% of TEP samples, respectively.

https://doi.org/10.5194/egusphere-2026-1873
Preprint. Discussion started: 10 April 2026

On average, a total air volume of 2.9 m^3 was sampled for hydrogels in SSA. Polycarbonate filters (25 mm, 0.2 µm pore size, Nucleopore, Whatman) were mounted in 47 mm polycarbonate filter housings including a silicon ring to bridge the filter size difference. Filters were flushed with air from the bubble chambers head space over the course of ~22 hours at a flow rate of ~ 2.2 L min^{-1}. The mean flow rate per filter was calculated by averaging the flow rates measured at the start and end of the collection period. Filters were stored in petri dishes at -20 °C until staining in the home laboratory. In total, single replicates collected on eight consecutive days have been analyzed (19.03.20-26.03.20). On the last day of the field campaign, the bubble chamber was supplied with MilliQ water to produce an operational blank. Additional blanks were taken before staining the aerosol filters as a control for the dyes. Aerosol particles were stained using a dual-staining approach to be able to approximate the contribution of CSP and TEP despite the limited availability of aerosol filters (details are provided in the supplementary information). This approach allows the distinction of TEP and CSP based on the color of each particle type, using only a single filter. In equivalence to their SSW precursors, the approximate contribution (CSP ratio in SSA*) of polysaccharide- and protein-containing hydrogels to total stainable aerosol particles could thus be assessed. Note that the abundance and size of SSA and SSW hydrogels were evaluated relying on the classical approach (Engel, 2009). In brief, aerosol particles retained on the filter were sequentially stained with 1 mL of Coomassie Brilliant Blue G working solution (stains protein-rich hydrogels) for 30 sec. After that, filters were rinsed three times with MilliQ water, air dried for a few minutes, and subsequently 1 mL of Alcian Blue working solution (stains acidic polysaccharides in carbohydrate-rich hydrogels) was applied, stained for five seconds, and rinsed with MilliQ water. Finally, filters were air dried and mounted on glass object slides using microscopy oil (refractive index 1.584, Cargille) and a coverslip, then frozen at -20 °C until the analysis. The operational blank was subtracted from the aerosol particles before the data analysis (absolute blank). The maximal equivalent spherical diameter (ESD) of the largest hydrogel in aerosols was 66 µm.

The abundance and size of SSA and SSW hydrogels were quantified by light microscopy at a magnification of x200. Image processing was conducted with Image J (*Image J*, 1.53a). From the area of single particles, their ESD is estimated indicating the size of the particles. The total particle abundance and area also include the largest particles, which measured 110 µm (TEP) and 162 µm (CSP) in size in comparison to the introduced size bins. Abundance of particles was grouped into five different size bins, including particles with an ESD>0.5 and <30 µm, and were summed up within the range of 0.5-1 µm (submicron), 1-2.5 µm, 2.5-5 µm, 5-10 µm, and 10-30 µm.

In comparison to hydrogels in SSW, the SSA collection on filters was conducted over a time period of 18.5 to 24 hours (Table A2), and only one replicate could be derived. Therefore, sample processing of the aerosol filters was adjusted by using the dual-staining approach, which enabled quantifying the approximate contribution of TEP-like and CSP-like aerosols on a single filter (CSP ratio in SSA*). Potential biases introduced by this adjustment in comparison to the seawater samples are discussed in the supplementary information.

https://doi.org/10.5194/egusphere-2026-1873
Preprint. Discussion started: 10 April 2026

2.3 Statistics

Statistics and plots were produced in R Studio (RStudio 2024.04.1+748). The data format represents the mean and standard deviation (M ± SD). Seawater and aerosol samples were tested for whether distribution patterns were normal (*Shapiro-Wilk* test) and homogeneous (*Levene's* test). For TEP and CSP, normality was not always given but for CSP even the assumption of homogeneity was violated. This violation was aggravated by exceptionally high particle numbers, which were collected on the 22nd and 23rd of March due to the presence of soot in the samples (Fig. 2a, b). As black particles interfere with the conducted microscopical analysis, these seawater samples were excluded from the statistical analysis of TEP and CSP in seawater. Otherwise, their inclusion is highlighted in the text and figures. The assumption of normality and homogeneity was also not met for certain parameters.

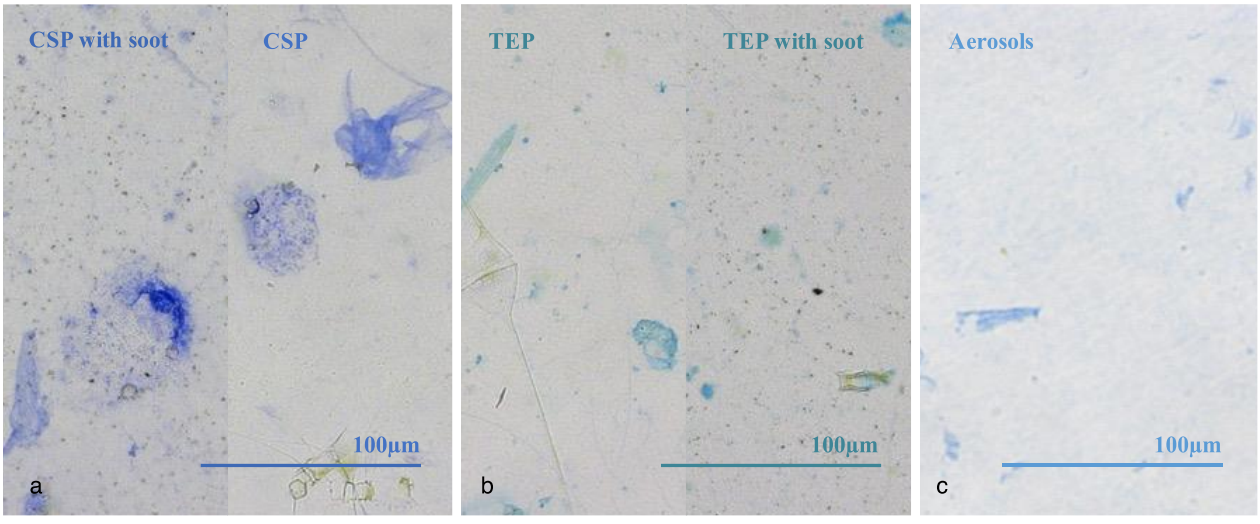

Figure 2 a) Examples of CSP and b) TEP samples with and without soot particles from sub-Antarctic Waters (SAW). c) An example of hydrogels in aerosols from the Subtropical Front (STF, 19.03.2020).

Enrichment factors (EF) were calculated and are based on the assumption that the concentration of a specific compound increases when it is transferred from, e.g. seawater into the air, and, therefore, the concentration in air was divided by the concentration in seawater (Equation 1).

$$EF = \frac{c_{(aer.\ hydrogels)}}{c_{(aer.\ Na^+)}} / \frac{c_{(wtr.\ hydrogels)}}{c_{(wtr.\ Na^+)}} \quad (1)$$

If the EF is smaller than 1, a depletion of the compound is encountered. It is necessary to introduce a tracer for seawater in air, i.e. sodium (Na^+), to be able to calculate the EF (Sander et al., 2003; Van Pinxteren et al., 2022). It was assumed that seawater contains 10 g Na^+ L^{-1} (Van Pinxteren et al., 2022). The amount of Na^+ in the filtered air was only assessed between the 19th and 24th of March 2020 and was on average 0.032 ± 0.015 µg m^{-3} (Tab. A2).

https://doi.org/10.5194/egusphere-2026-1873
Preprint. Discussion started: 10 April 2026

The size distribution of hydrogel particles can be described by

$$\frac{dN}{d(d_P)} = kd_P^{\delta} \quad (2)$$

the change in the abundance of particles per unit of volume (dN) over the respective ESD size class (d_P) to ($d_P + d(d_P)$). The constant k is dependent on the concentration of particles and the exponent δ describes the size distribution ($\delta < 0$). Based on a linear regression fitted on log-log scale transformed data, the characteristic spectral slope δ can be determined (Engel, 2009). A shallower spectral slope indicates a relatively higher fraction of larger particles, while a steep slope indicates relatively high fractions of small versus relatively few large particles.

To evaluate if the regimes and the time of the day had an effect on TEP and CSP abundance, area, and size-distribution or on the biological variables, a non-parametric multifactorial *ANOVA* (aligned rank transformed ANOVA, Wobbrock et al., 2011) was conducted (package *ARTool*, command applied 'art'), accounting for the inconsistent nature of normality and heterogeneity in the sample set. Represented by a 'heatmap', the potential influence of biogeochemical parameters on hydrogels in seawater and air was assessed. Complying with the distribution of the data, Spearman rank correlations were applied to build the heatmaps. CSP and TEP, excluding soot samples, were compared to the biogeochemical data set of the corresponding sampling time, i.e., 8:00 AM and 4:00 PM. For the comparison of seawater data with hydrogels in SSA, bulk data were pooled to derive a mean over the time of aerosol generation, including an afternoon (4:00 PM) and next-morning sample (8:00 AM), including seawater samples influenced by soot. Aerosol collection started normally around 11:00 AM and finished the next day around 9:00 AM (sampling duration between 18.5 and 24 hours).

3 Results

Hydrogel abundance in surface sea waters (SSW) and sea spray aerosols (SSA) was investigated across four distinct oceanic regimes, including the subantarctic (SAW, n=6), and subtropical waters (STW, n=2). In the subtropical front (STF), phytoplankton blooms occur year-round based on the available micro- and macronutrients (n =8). Another productivity regime resulted from the mixing of STW and the waters of the Cook Strait (MIX, n=4) (Fig. 1). The filtration of particulate material revealed sporadic 'black filter' events in the SAW, which seem related to the Australian bushfires as the satellite CALIPSO confirmed the presence of ash clouds above the tropopause in the sampling region. In the morning of the 22nd, we also experienced heavy rainfall. Black particles between 0.5 and 2.5 µm in size were present in CSP and TEP samples on the 22nd and 23rd of March in the afternoon. Black particles occurred only in the seawater samples (Fig. 2a, b), while the aerosol filters seemed unaffected (Fig. 2c).

https://doi.org/10.5194/egusphere-2026-1873
Preprint. Discussion started: 10 April 2026

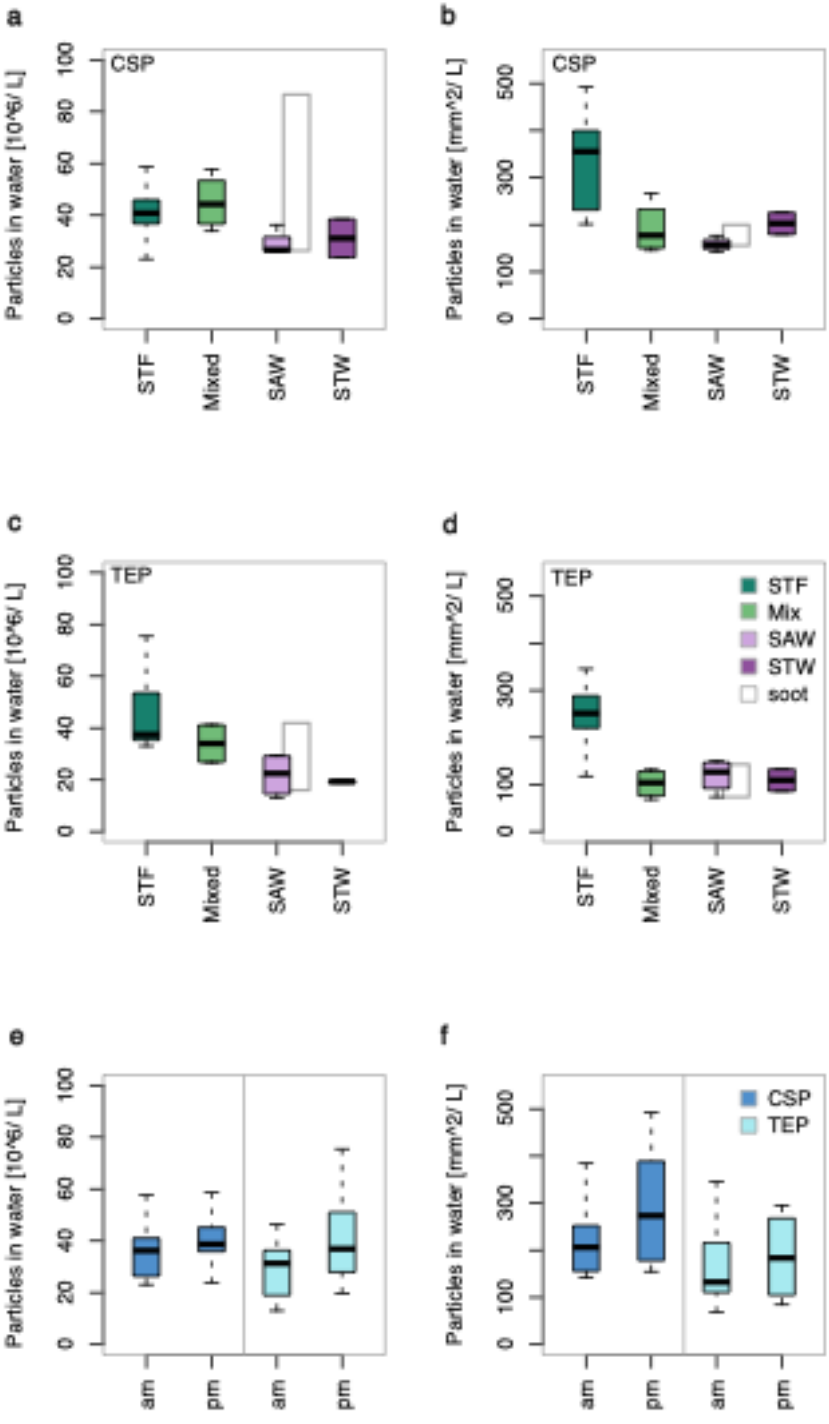

Figure 3 a, b) Protein-rich hydrogels (Coomassie stainable particles, CSP) abundance and area and c, d) carbohydrate-rich hydrogel (transparent exopolymer particles, TEP) abundance and area in sea surface water grouped into four productivity regimes, which are represented by different colours corresponding to the Subtropical front (STF), sub-Antarctic Waters (SAW), Subtropical waters (STW), and a mixed regime (MIX). Black lines represent the mean. The grey box represents SAW data in which samples with soot-influenced particles are included. The size of the box corresponds to the inner two quantiles. e, f) The change of CSP and TEP abundance and area observed between morning (am) and afternoon (pm) stations, including soot particles.

https://doi.org/10.5194/egusphere-2026-1873
Preprint. Discussion started: 10 April 2026

3.1 Hydrogels in surface seawater

CSP abundance was highest in the MIX (45 ± 11 × 10^6 L^{-1}) and the STF (41 ± 11 × 10^6 L^{-1}) decreasing to on average 29 ± 5 × 10^6 L^{-1} in the SAW and to 31 ± 11 × 10^6 L^{-1} in the STW (Fig. 3a). However, the difference between regimes was only statistically significant for total CSP area (art ANOVA, p-value<0.001, results are summarized in Table A3). While CSP area reached 333 ± 103 mm^2 L^{-1} in the STF (contributing 57 ± 7% to total hydrogel area), it declined to a minimum of 158 ± 14 mm^2 L^{-1} in the SAW (58 ± 8%), and was only slightly higher in the MIX (191 ± 55 mm^2 L^{-1}, 65.4 ± 2.8%) and STW (202 ± 33 mm^2 L^{-1}, 65 ± 3%) (Fig. 3b; Table A4). Particles >5 µm were responsible for the significant difference in CSP area across regimes. The size distribution of particles, factorized as the spectral slope (δ), shifted across regimes from the shallowest slope characterizing the STF (-2.35 ± 0.18) (where the fraction of large particles was high) to the steepest slope in the MIX (-2.68 ± 0.15) (where the fraction of smallest particles was high). The ratio of CSP area to the total area of hydrogels (CSP+TEP) in SSW changed between regimes, however, was only significantly different for the smallest (0.5-1 µm) and largest (10-30 µm) size bin. In contrast to CSP, TEP abundance changed significantly across regimes (art ANOVA, p-value=0.023). The highest TEP abundance was found in the STF (45 ± 15 × 10^6 L^{-1}), followed by the MIX (34 ± 8 × 10^6 L^{-1}), and was lowest in the SAW (22 ± 9 × 10^6 L^{-1}) and STW (19 ± 1 × 10^6 L^{-1}; Fig. 3c). The total area of TEP differed significantly across regimes (art ANOVA, p-value=0.005; Fig. 3d). In the STF, TEP area was drastically larger (248 ± 67 mm^2 L^{-1}) than in all other regimes. In the SAW, TEP area was 120 ± 35 mm^2 L^{-1}, while in the STW and MIX, TEP area diminished further to 109 ± 33 and 102 ± 31 mm^2 L^{-1}, respectively. TEP of all size bins contributed to the differences in abundance and area observed across regimes. The shift in size spectrum indicated as slope (δ) was likewise significant, yielding the shallowest slope in the STF (-2.37 ± 0.15) and STW (-2.39 ± 0.07), an intermediate slope in the SAW (-2.47 ± 0.04) and the steepest within the MIX (-2.71 ± 0.08) (art ANOVA, p-value=0.016).

It was further explored whether the time of day affected particle abundance and area. CSP area increased significantly over the course of the day (AM: 214 ± 74 mm^2 L^{-1}; PM: 291 ± 129 mm^2 L^{-1}) (art ANOVA, p-value=0.039; Fig. 3e, f), while CSP abundance showed no effect. Larger size bins (2.5-10 µm) contributed significantly to the shift observed in CSP area. Only by trend, an increase in TEP abundance and area was detected over the course of the day (AM: 160 ± 87 mm^2 L^{-1}; PM: 187 ± 87 mm^2 L^{-1}) (Fig. 3e). In contrast to CSP, the shift in TEP area was mainly controlled by particles smaller than 2.5 µm in size. By tendency, the spectral slope of CSP shifted towards larger hydrogels in the afternoon (AM: -2.50 ± 0.16; PM: -2.43 ± 0.24), while TEP seemed to become slightly more fragmented during the course of the day (AM: -2.46 ± 0.16; PM: -2.49 ± 0.20; Table A4). The averaged ratio of CSP to TEP area increased accordingly, however, yielding insignificant results (AM: 59 ± 8%; PM: 61 ± 5%).

https://doi.org/10.5194/egusphere-2026-1873
Preprint. Discussion started: 10 April 2026

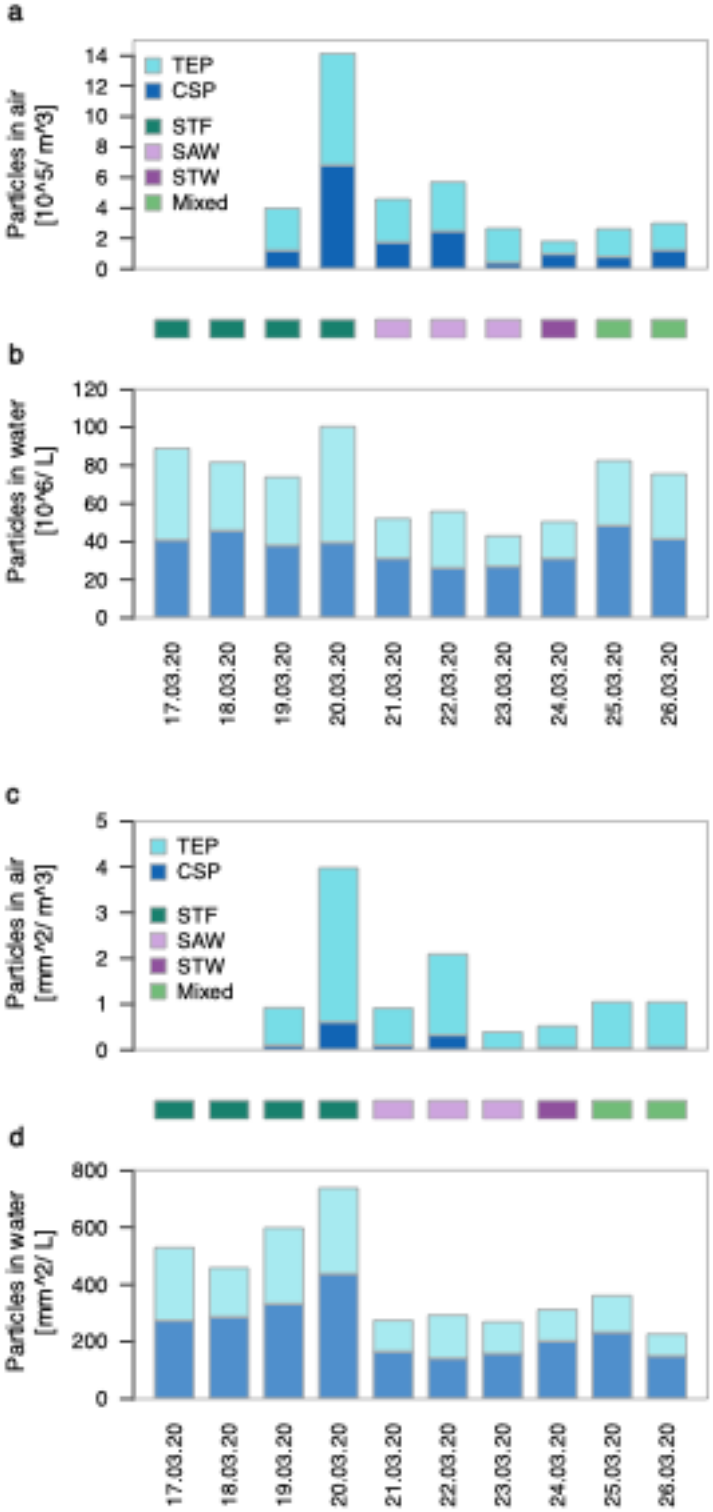

Figure 4 The daily averaged abundance of hydrogels a) in sea spray aerosols (SSA) and b) surface seawater (SSW) grouped into carbohydrate- (TEP, light blue) and protein-rich (CSP, dark blue) particles. The daily averaged area of hydrogels c) in SSA and b) SSW grouped into TEP and CSP. Coloured boxes represent four different regimes, i.e., the Subtropical front (STF), sub-Antarctic Waters (SAW), Subtropical waters (STW), and a mixed regime (MIX). Samples collected on the 22rd and 23th of March were potentially influenced by soot. Abbreviations: Transparent exopolymer particles (TEP), Coomassie stainable particles (CSP).

https://doi.org/10.5194/egusphere-2026-1873
Preprint. Discussion started: 10 April 2026

3.2 Hydrogels in sea spray aerosols

SSA hydrogel abundance and area varied greatly along the cruise track. Due to the limited sample size, no statistical tests were performed. SSA hydrogel concentration ranged from 0.9 ± 0.7 × 10^5 m^{-3} (n=2) in the STF to 0.2 × 10^5 m^{-3} in the STW (n=1). Intermediate concentrations characterized the SAW and MIX (Fig. 4a, results are summarized in Table A3). The fraction of CSP number in aerosols was largest in the STW (53%) and smallest on the 23rd of March in the SAW (15%). On average, SSA hydrogel area was largest in the STF (2.5 ± 2.2 mm^2 m^{-3}), intermediate in the SAW (1.1 ± 0.9 mm^2 m^{-3}) and MIX (1.1 ± 0.0 mm^2 m^{-3}), diminishing to 0.5 mm^2 m^{-3} in the STW (Fig. 4b). The fraction of CSP area in aerosols was considerably smaller than the fraction of TEP, reaching its maximum in the STF on the 22nd of March (15%) and its minimum in the MIX on the 25th of March (4%). Proteinaceous particles were thus predominantly present in the smaller size bins. Figure 5 shows the fractions of CSP and TEP contributing to overall abundance across equivalent size bins for SSA and SSW. In the SSW samples, CSP to TEP ratios varied only slightly between all size bins (CSP: 55 ± 9%). The variability in SSA hydrogels was higher (CSP: 38 ± 12%) and exhibited a clear pattern. CSP contributed especially to the smallest size bin (0.5-1 µm; 45 ± 12%), and decreased continuously, reaching its minimum in the largest size bin (5-10 µm; 9 ± 11%). SSA hydrogel abundance was on average 0.22 ± 0.21 × 10^5 m^{-3} in the smallest size bin (0.5-1 µm) and declined by one order of magnitude to 0.14 ± 0.07 × 10^4 m^{-3} in the largest represented size bin (5-10 µm) (Table 1).

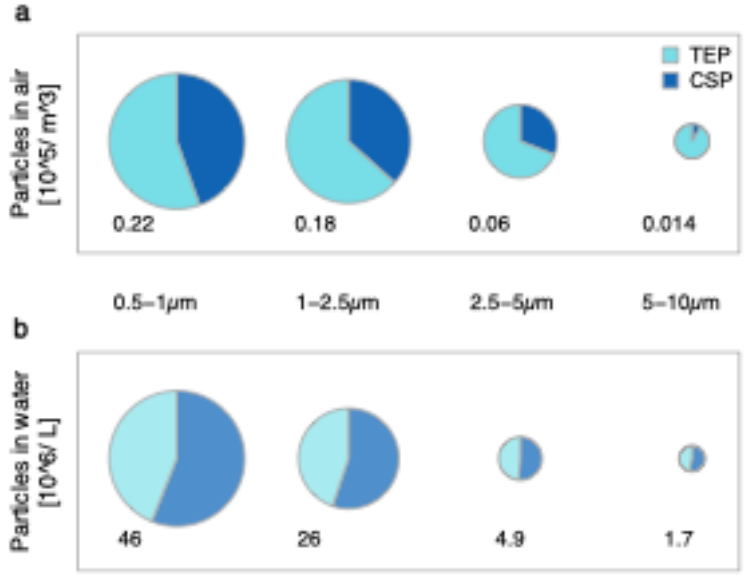

Figure 5 Protein-rich (Coomassie stainable particles, CSP) and carbohydrate-rich (transparent exopolymer particles, TEP) hydrogel abundance in sea spray aerosols (SSA, in air) and surface seawater (in water). The area of circles is relative to the abundance of hydrogels assessed in the respective size bins, which only include particles with an equivalent spherical diameter of 0.5 to 10 µm. Abundances are additionally indicated below each circle. It should be noted that the concentration of hydrogels in water and air referrers to different units of volume, and, therewith the enrichment in aerosols relative to seawater is not adequately depicted. Only SSW samples (n=15) collected during the days in which aerosol filters were generated (n=8) are included.

Table 1 Particle abundance of hydrogels, CSP abundance ratio to total hydrogel particle abundance, and the enrichment factors grouped into size bins. Abbreviations: Transparent exopolymer particles (TEP), Coomassie stainable particles (CSP), surface

https://doi.org/10.5194/egusphere-2026-1873
Preprint. Discussion started: 10 April 2026

seawater (SSW, n=15), sea spray aerosols (SSA, n=8). The table summarizes the data presented in Fig. 5. Only SSW samples collected during the days in which aerosol filters were generated are included. Within the smallest size bins (0.5-2.5 µm), included soot samples (n=2) may marginally bias the here represented results. To approximate the CSP area in SSA, an alternative staining method was applied (*, Supplementary Information).

Size bins	**0.5-1 µm**	**1-2.5 µm**	**2.5-5 µm**	**5-10 µm**
Data format	[mean ± SD]	[mean ± SD]	[mean ± SD]	[mean ± SD]
TEP in SSW [× 10^6 L^{-1}]	21 ± 12	12 ± 8	2.4 ± 0.8	0.8 ± 0.4
CSP in SSW [× 10^6 L^{-1}]	25 ± 12	14 ± 8	2.5 ± 0.8	0.9 ± 0.4
CSP ratio in SSW [%]	56 ± 12	55 ± 7	51 ± 6	54 ± 7
Hydrogels in SSA [× 10^3 m^{-3}]	22 ± 21	18 ± 13	6.3 ± 4.8	1.4 ± 0.7
CSP ratio in SSA* [%]	45 ± 12	37 ± 13	31 ± 26	9 ± 11
Enrichment factor [× 10^5]	2.2 ± 2.4	3.1 ± 3.1	5.0 ± 5.1	2.9 ± 1.9

As SSA hydrogel concentration was calculated by referring to the volume of filtered air, sodium (Na^+) can be introduced as a conservative tracer to track the equivalent amount of SSW which was transferred into the air (Van Pinxteren et al., 2022). Absolute SSA concentration in relation to transferred Na^+ were highest in the STF (4.1 ± 2.1 × 10^3 hydrogels ng^{-1} Na^+), followed by the SAW (1.5 ± 0.7 × 10^3 hydrogels ng^{-1} Na^+) and decreased to a minimum in the STW (0.4 × 10^3 hydrogels ng^{-1} Na^+). Sodium concentrations for the MIX regime are not available. SSA abundance grouped into size bins and set in relation to emitted Na^+ reflected the previously introduced results (n=6): 1.0 ± 1.0 × 10^3 hydrogels ng^{-1} Na^+ were emitted in the smallest bin (0.5-1 µm), 0.8 ± 0.7 × 10^3 hydrogels ng^{-1} Na^+ in the first intermediate (1-2.5 µm), 0.3 ± 0.2 × 10^3 hydrogels ng^{-1} Na^+ in the second intermediate (2.5-5 µm), and 0.06 ± 0.04 × 10^3 hydrogels ng^{-1} Na^+ in the largest size bin (5-10 µm). Furthermore, the enrichment of SSA hydrogels in relation to SSW can be calculated by referring to Na^+, yielding a mean EF of 2.7 ± 2.8 × 10^5 for samples derived between the 19th and the 24st of March (n=6). Enrichment was highest in the STF (5.3 ± 3.9 × 10^5), and smallest in the STW (0.5 × 10^5), while for the MIX data are not available. Enrichment varied when grouped into the size bins, yielding the highest EFs in an intermediate size bin 2.5-5 µm (5.0 ± 5.1 × 10^5), while decreasing to a minimum of 2.2 ± 2.5 × 10^5 (0.5-1 µm) in the smallest size bin. Intermediate sized hydrogel particles (1-5 µm) became thus preferably enriched during bubble bursting (Table 1). The shallower slope of the SSA size spectrum (δ=-1.97 ± 0.19) in comparison to relevant SSW samples (CSP δ=-2.53 ± 0.25; TEP δ=-2.54 ± 0.23, including soot samples) describes the same phenomenon. A comparison between SSA and relevant SSW samples yielded significant differences in size spectra (δ), no matter whether SSW soot samples were included or excluded (art ANOVA, *p*-value<0.001). The SSA enrichment factor for total hydrogel area becomes extremely small (1.9 ± 2.2) when including all hydrogel particles as hydrogels in the SSW were much larger (max. ESD: 110 µm for TEP and 162 µm for CSP) than in SSA (max. ESD: 66 µm).

https://doi.org/10.5194/egusphere-2026-1873
Preprint. Discussion started: 10 April 2026

3.3 Biogeochemical characteristics

To assess the impact of the biogeochemical regime on the emission of hydrogels in SSA and the abundance of CSP and TEP in SSW, the next paragraph will describe the abundance of bacterio- and phytoplankton and the composition of organic matter (summarized in Table A3). Regimes were characterized by specific changes, which have been partly introduced before (Sellegri et al., 2023; Barthelmeß et al., 2025). Presented abundances of microorganisms and concentrations of organic matter can differ slightly as only morning and afternoon samples were included in this analysis in alignment with the collection of SSW TEP and CSP samples. Total chlorophyll a (Chl *a*) concentration was highest in the STF (2.06 ± 0.79 mg m^{-3}), intermediate in the MIX (0.82 ± 0.24 mg m^{-3}), and decreased to lowest concentrations in the STW and SAW (0.36 ± 0.05 mg m^{-3}) (art ANOVA, p-value<0.001). Overall, Chl *a* grouped into size fractions followed a decreasing order of rank in concentration (STF>MIX>STW>SAW) with one exception: The largest Chl *a* fraction (cells >20 µm) exhibited minimal concentrations in the STW. Eukaryotic picophytoplankton (0.2-2 µm) and *Synechococcus* spp. reached maximal abundance in the MIX, however, differences between regimes were insignificant. Nanophytoplankton (2-20 µm) significantly characterized regimes as they were most abundant in the STF (2.31 ± 0.45 × 10^3 mL^{-1}), only half as abundant in the SAW (1.26 ± 0.62 × 10^3 mL^{-1}), and diminished in the STW (0.84 ± 0.05 × 10^3 mL^{-1}) and MIX (0.81 ± 0.38 × 10^3 mL^{-1}) (art ANOVA, p-value<0.001). Bacteria exhibited maximal abundances in the STF (3.02 ± 0.46 × 10^6 cells mL^{-1}) and MIX (3.00 ± 0.98 × 10^6 cells mL^{-1}), and similar low abundances in the SAW and STW (1.87 ± 0.43 × 10^6 cells mL^{-1}) resulting in significant changes across regimes (art ANOVA, p-value=0.020). TOC and TON reached highest concentrations in the STF (TOC: 88.7 ± 10.4 µM; TON: 8.35 ± 1.40 µM), intermediate concentrations in the STW then MIX, and minimal concentrations in the SAW (TOC: 70.4 ± 2.4 µM; TON: 5.35 ± 1.36 µM). The difference in TOC and TON across regimes was significant (art ANOVA, p-value<0.001). PAA and PCCHO concentration followed a distributional pattern which was comparable to Chl *a* concentration. Again, the change across regimes was significant for both parameters (art ANOVA, p-value=0.001). As presented in Barthelmeß et al., (2025), the concentration of DAA and DCCHO did not necessarily follow the distributional pattern of their particulate fractions. Degradation indices derived from DAA concentrations (DAA-C yield) and composition (DI) (Davis et al., 2009; Davis & Benner, 2007) were highest in the MIX (DAA-C yield: 2.31 ± 0.62%) and STF (DI: 0.93 ± 2.68), respectively, intermediate in the SAW, and lowest in the STW (DAA-C yield: 1.47 ± 0.11; DI: -2.63 ± 2.05) when including morning, afternoon and night-time samples (Barthelmeß et al., 2025).

https://doi.org/10.5194/egusphere-2026-1873
Preprint. Discussion started: 10 April 2026

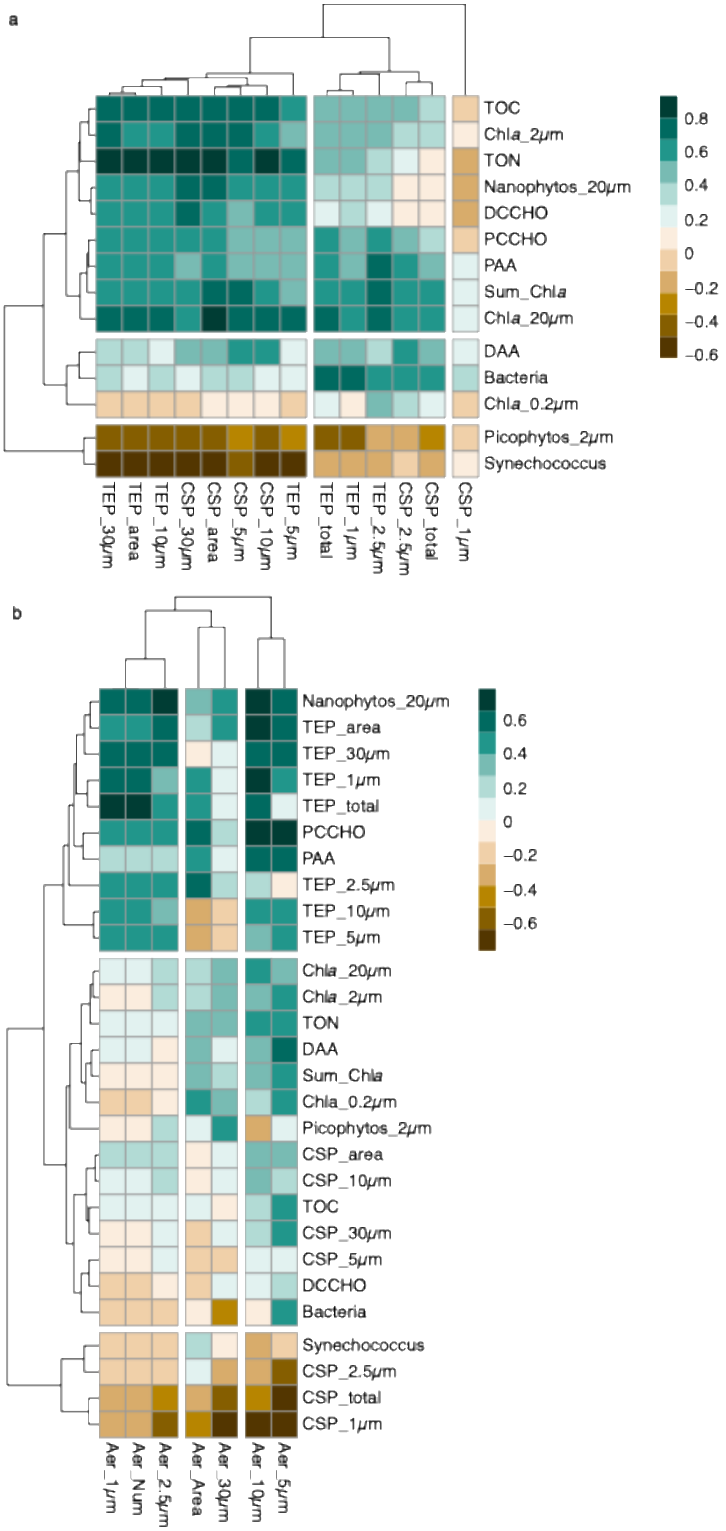

Figure 6 Spearman rank correlation matrix of biogeochemical parameters with protein- and carbohydrate-enriched hydrogel abundance a) in surface seawater and b) in sea spray aerosols grouped into size bins. Positive correlations are depicted in green and negative correlations are depicted in brown and as annotated by the legends. Abbreviations: total organic carbon (TOC), chlorophyll *a* (Chl*a*) in the corresponding size bin or their sum, total organic nitrogen (TON), dissolved and particulate combined carbohydrates (D/PCCHO), dissolved and particulate amino acids (D/PAA), picophytoplankton abundance (Picophytos) and nanophytoplankton abundance (Nanophytos) as assessed by flow cytometry. Transparent exopolymer particles (TEP) which are composed of carbohydrate-rich material, Coomassie stainable particles (CSP), which are composed of protein-like material. TEP and CSP are either indicated in abundance including the respective size-bin (0.5µm-10µm) or their sum (total), or their total area (area). Aerosolized hydrogels (Aer) abundances are likewise assigned to their respective size-bins, or total abundance (Num), or area.

https://doi.org/10.5194/egusphere-2026-1873
Preprint. Discussion started: 10 April 2026

3.4 Biogeochemical factors influencing hydrogel occurrence in seawater and aerosols

The correlation matrices describe potential dependencies of CSP and TEP in SSW (Fig. 6a) and hydrogels in SSA (Fig. 6b) with biogeochemical parameters with a strong focus on biological components. The correlations with biogeochemical parameters were generally weaker for smaller particles, i.e. total CSP and TEP abundance in particular defined by the smallest particles in the range of 0.5-2.5 µm. Exceptions existed as e.g., smallest particles exhibited stronger correlations with bacterial abundances in comparison to larger particles (2.5-30 µm), and TEP (1-2.5 µm) correlated well with Chl *a* (cells >20 µm) and total Chl *a* concentration. Opposing the trend in all further hydrogel classes, the smallest CSP bin (0.5-1 µm) was characterized by slightly negative correlations with almost all biogeochemical factors presented. Larger size classes (2.5-30 µm) and the total area of CSP and TEP were characterized by overall strong positive correlations. TON, Chl *a* (cells >20 µm), and TOC correlated best with the occurrence of the largest hydrogels. Nanophytoplankton abundance was the only microbial factor which correlated positively with larger sized TEP and CSP (2.5-30 µm). The strongest negative correlations of intermediate and large hydrogels were defined by *Synechococcus* spp., eukaryotic picophytoplankton abundance, and the concentration of Chl *a* (cells >0.2µm).

Hydrogels in SSA clustered again according to their sizes (Fig. 6b). In general, most TEP size classes along with nanophytoplankton abundance positively correlated with SSA hydrogel abundance across all size classes. SSA hydrogels correlated negatively with factors describing the smallest planktonic organisms, in particular heterotrophic bacteria and *Synechococcus* spp., but also with smallest CSP (0.5-2.5 µm) and, consequently, CSP number.

4 Discussion

4.1 Biogeochemical drivers of hydrogels in surface seawater

Hydrogel number and area are recognized to vary greatly across oceanic regimes and depths (Engel et al., 2020). In general, CSP and TEP area is greatest in the surface ocean and at sites of elevated primary production (e.g. in the Eastern Boundary Upwelling Systems; CSP: 290 $mm^2\ L^{-1}$, TEP: 259 $mm^2\ L^{-1}$), while concentrations may diminish in the open ocean e.g., in the subtropical South Pacific (equivalent to the STW; TEP: 8 $mm^2\ L^{-1}$) (Engel et al., 2020). Here, CSP and TEP area was maximal in the STF (CSP: 333 $mm^2\ L^{-1}$, TEP: 247 $mm^2\ L^{-1}$) and declined to its minima in an open ocean regime and mixed waters (e.g. SAW, CSP: 158 $mm^2\ L^{-1}$; MIX, TEP: 102 $mm^2\ L^{-1}$). CSP and TEP areas sampled during our campaign thus reflected the upper global range in surface hydrogel variability. The number, composition, and size distribution of marine hydrogels are influenced by multiple factors, which are sometimes difficult to disentangle. CSP and TEP formation have been frequently associated with high Chl *a* concentration (Cisternas-Novoa et al., 2015; Engel et al., 2017, 2020; Zamanillo et al., 2019). However, the production rate of CSP and TEP generally depends on the phytoplankton community (Cisternas-Novoa et al., 2015; Engel et al., 2017) and environmental stressors such as nutrient deficiencies (Engel et al., 2004; Myklestad, 1995). For example, it was

https://doi.org/10.5194/egusphere-2026-1873
Preprint. Discussion started: 10 April 2026

shown that TEP production was enhanced in a diatom-dominated experiment in contrast to prokaryotic *Synechoccocus* spp. cultures, in which CSP production prevailed (Cisternas-Novoa et al., 2015). In eukaryotic phytoplankton cultures (*G. huxleyi)*, TEP production increased considerably under nutrient stress (Engel et al., 2004). In agreement, highest TEP abundance and area characterized the STF, which aligns well with highest Chl *a* concentration. An elevated Chl *a* concentration is representative of this region as the convergence of macro- and micronutrient replenished waters above the Chatham Rise favors the formation of phytoplankton blooms year-round (Law et al., 2017; Murphy et al., 2001). Under the dominance of large diatoms (Sellegri, Harvey, et al., 2023), TEP also contributed a relatively large fraction of total hydrogel area (43%). Chl *a* concentration was still elevated in the MIX waters, although mainly reflecting the presence of picophytoplankton dominated by prokaryotic *Synechococcus* spp. Here, a slight reduction in TEP abundance but slightly higher CSP abundance in comparison to the STF occurred. TEP area declined drastically (35%) in relation to total hydrogel area. Both sites, the STF and MIX, are representative of nutrient replenished regimes, which harbored a diverse phytoplankton community (Sellegri, Harvey, et al., 2023), and highest bacterial abundances. This was also indicated by high amino acid degradation indices, suggesting that the DAA pool is replenished by fresh phytoplankton products relative to the STW and SAW (Barthelmeß et al., 2025). Tentatively, elevated *Synechococcus* spp. abundance could account for the relative enrichment of CSP area and in alignment with the results of Cisternas-Novoa et al., 2015.

TEP but also CSP abundance were lowest in the nutrient-deficient regimes (SAW and STW), which were characterized by minimal Chl *a* concentration, bacterial abundance, and degradation indices. Although both regimes are marked by nutrient deficiencies, they represent contrasting trophic conditions (Moore et al., 2013). In the SAW, micronutrients such as iron are scarce and, consequently, limit the uptake of macronutrients such as nitrogen, which can not be incorporated into intracellular biomass (Chien et al., 2023) and therewith do neither contribute to extracellular organic material. This is mirrored by minimal CSP area (158 mm^2 L^{-1}), TOC and TON concentrations but also a relatively reduced contribution of CSP to overall hydrogel area in the SAW (58%, comparable to the STF). The opposite is true for the STW, in which micronutrients are replenished. In this regime, scarce macronutrients can be supplied by microbial atmospheric nitrogen fixation and are readily incorporated into biomass (Chien et al., 2023; Wang et al., 2019). This is in agreement with the observed intermediate CSP area (202 mm^2 L^{-1}), TOC and TON concentrations in the STW, where CSP contributed 65% to the total area of hydrogels (comparable to the MIX regime).

Regimes characterized by the highest relative and absolute TEP area (STF, SAW) had elevated nanophytoplankton abundance in common, while in regimes characterized by the lowest relative and absolute TEP area, equally low nanophytoplankton cells occurred (MIX, STW). Eukaryotic phytoplankton taxa, such as diatoms or dinoflagellates, often form in mutually beneficial relationships with marine bacteria. Organic carbon is exchanged with nutrients such as iron, vitamins, or ammonia (Amin et al., 2009, 2015; Durham et al., 2015). This trade is accomplished in the phytoplankton's 'phycosphere', an extracellular gel-like matrix composed of TEP, which is inhabited by bacteria (Bell & Mitchell, 1972; Seymour et al., 2017; Sperling et al.,

https://doi.org/10.5194/egusphere-2026-1873
Preprint. Discussion started: 10 April 2026

2017). Moreover, cell-associated, large and acidic polysaccharides excreted by phytoplankton enhances iron bioavailability in the Southern Ocean (Amin et al., 2015; Hassler et al., 2011). Therefore, nutrient-deficiencies may strengthen mutually beneficial microbial relationships aside TEP formation in the SAW.

However, hierarchical clustering revealed that the size distribution, rather than subtle compositional differences of hydrogels, corresponded best to biogeochemical conditions (as depicted by cluster groupings in Fig. 6a). An elevated Chl *a* concentration, particularly of larger phytoplankton cells (>2 µm), in concert with elevated TON, TOC, DCCHO concentration, and nanophytoplankton abundance favored the occurrence of larger CSP and TEP hydrogels. Contrastingly, correlation statistics were poor for small CSP in particular but also small TEP (<1 µm). Other factors must have shaped hydrogel occurrence in this range. Shorter polymers assemble to rather short-lived, small hydrogels and originate from the refractory, photochemically altered DOC pool. In comparison, larger hydrogels are derived from undegraded, long i.e., freshly produced polymers (Passow, 2000; Orellana & Verdugo, 2003; Verdugo, 2012), which contain an elevated fraction of acidic sugars (Borchard & Engel, 2015; Hassler et al., 2011; Hoagland et al., 1993). While large hydrogels are therefore clearly aligned with phytoplankton abundance pattern and fresh production, they reflect conditions in which larger, eukaryotic phytoplankton cells thrive. Usually, this corresponds to more productive regimes. Smaller hydrogels, in contrast, may assemble and decompose stochastically, which would explain the weak correlations obtained with biogeochemical factors.

4.2 Absolute and relative concentration of hydrogels depends on biogeochemical regimes

To the best of our knowledge, we are the first to present data on the concentration of hydrogels in SSA above characteristic regimes of the Southern hemisphere oceans. Highest hydrogel concentrations in relation to Na^+ were detected in the STF (4.1 ± 2.1 × 10^3 hydrogels ng^{-1} Na^+), while the lowest concentration was measured in the STW (0.4 × 10^3 hydrogels ng^{-1} Na^+), therewith varying by one order of magnitude across biogeochemical regimes and corresponding to highest and lowest biological activity, respectively. This aligns well with previous findings in which aerosol emission was pronounced above productive oceanic regions scaled with satellite-derived Chl *a* concentration (Long et al., 2014; O'Dowd et al., 2015; O'Dowd et al., 2004). Aller et al. (2017) reported TEP and CSP as fractions of total particle mass, contributing approx. 1 to 100% of total particle mass in SSA. Aller et al. (2017) is the only study that has previously examined both TEP and CSP in SSA, however, data are not directly comparable as methods, including SSA generation and the quantification of hydrogels, differed. While they quantified TEP and CSP using a colorimetric technique, expressed in xanthan gum (XG) and bovine serum albumin (BSA) equivalents, respectively, we instead applied a microscopic approach. In the SSW, TEP concentration in µg XG equiv. L^{-1} usually corresponds to TEP area expressed in mm^2 L^{-1} (Dreshchinskii and Engel., 2017). In our study, hydrogel area in SSA ranged from 0.5 to 4.0 mm^2 m^{-3} (Fig. 4c), which would translate to equivalent concentrations in µg m^{-3}, assuming the same relationship holds as in SSW. In alignment with our results, Aller et al. (2017) detected 2 to 14 µg XG and BSA equiv. m^{-3} in SSA. Van Pinxteren et al. (2022) reported that TEP (>4.5 µm) concentration in ambient marine aerosols were in average

https://doi.org/10.5194/egusphere-2026-1873
Preprint. Discussion started: 10 April 2026

2.5 hydrogels ng^{-1} Na^+ (as approximated based on their supplementary information, Table S2), which is comparable in magnitude to our results obtained for the largest size-bin (5-10 µm; 60 hydrogels ng^{-1} Na^+).

We further identified carbohydrate-like hydrogels as the main component in aerosols (submicron: 55%; supermicron: 75%). In equivalence, organic mass in submicron ambient marine aerosols was dominated by carbohydrate-like material accounting for 47-61%, and was enriched by a factor of 10^3 to 10^4 in relation to SSW in pristine oceanic air masses above the Arctic and North Atlantic Ocean (Russell et al., 2010). Submicron SSA, which were generated from continuously supplied North-Eastern Atlantic water deploying a plunging-jet system, were likewise enriched in carbohydrates and enriched by a factor of 10^5 in comparison to SSW concentrations (Rastelli et al., 2017). On average, Van Pinxteren et al. (2022) calculated an enrichment of $0.9\text{-}2.0 \times 10^4$ for carbohydrate-like hydrogels in ambient marine aerosols. In our study, the EF (including all particle sizes and types) was on average $2.7 \pm 2.8 \times 10^5$. Therewith, concentration and enrichment aligns reasonably well with the reported range in the literature.

It has been previously observed that carbohydrate-like material and sea salt concentration in aerosols strongly correlated with wind speed, linking aerosol production to the ocean and bubble intrusion and scavenging by wind forcing (Russell et al., 2010). Immersed bubbles scavenge the underlying bulk and drag TEP along and/ or introduce an attraction based on physicochemical properties, explaining the selective enrichment of hydrogels in the SML (Robinson et al., 2019), but also in aerosols (Van Pinxteren et al., 2022). Kuznetsova et al. (2005) further described the phenomenon that relatively larger hydrogels were enriched in aerosols in comparison to the SSW, which is in alignment with the here reported difference in size-dependent spectral slopes of SSA and SSW hydrogels. A redistribution towards larger particles in aerosols was also apparent for dissolved organic matter, which assembled into new particles during the process of bubbling (Kuznetsova et al., 2005). We agree with the authors that, given a mere physical transfer of SSW precursors, one would expect a similar size distribution of hydrogels in SSA and SSW precursors (Kuznetsova et al., 2005). New particles form at bubble surfaces during their rise due to the adsorption of surface-active polymers, which become compressed and aggregate into a cap at its rear (Dukhin et al., 2015). Furthermore, colloids or small microgels easily assemble into larger hydrogels upon collision (Verdugo et al., 2004). Therefore, a size shift from seawater to the SML (Galgani et al., 2016; Silva et al., 2025) but also SSA is not surprising given the physical forcing introduced by bubbling. An alternative, method-based explanation is that the relatively larger hydrogels encountered in seawater could break into smaller fragments during the splashing process induced by the plunging-jet system.

In addition to changing absolute hydrogel concentration above the regimes and a general size shift from SSW precursors to SSA hydrogels, we also observed that the relative enrichment was pronounced or diminished above the STF and STW, respectively. Therefore, enrichment likely further corresponds to the organic matter composition encompassed in the SSW. TEP was the marine precursor species that best predicted hydrogel concentration (Fig 6b). As discussed in section 4.1, larger polymers facilitate TEP aggregation, while smaller polymers assemble and disperse stochastically. This also became apparent

https://doi.org/10.5194/egusphere-2026-1873
Preprint. Discussion started: 10 April 2026

within a bubble scavenging experiment: Highly surface-active carbohydrates of freshly released phytoplankton biomass were rapidly scavenged from the water column, leaving behind polymers less prone to aggregate, until TEP production ultimately ceased after a few hours of bubbling (Zhou et al., 1998). Conclusively, bubbling scavenges, up-concentrates and aggregates precursors more efficiently into aerosols in regimes in which freshly produced, large polymeric carbohydrates occur. This also explains the quite similar concentration and enrichment pattern observed within the SAW and MIX, as the SAW was characterized by elevated TEP area, and relatively larger particles (size-dependent spectral slopes) in comparison to the MIX. It should be emphasized that this was the case despite higher Chl *a*, TON, TOC, PCCHO and PAA concentrations in the MIX regime. Although averaged hydrogel concentration and enrichment in SAW aerosols were slightly elevated in comparison to the MIX, they greatly varied within the three monitored days. It should be further considered that the cruise-track crossed SAW waters, which were impacted by heavy rain (second day in the SAW) and soot emanating potentially from the Australian bushfires (second and third day in the SAW). Soot and fine coal dust are examples of hydrophobic particles, which are related to foam destabilization, aggregate formation, and aggregate sinking induced by ballasting (Fan et al., 2004; Jenkinson et al., 2018; Mari et al., 2014). While soot particles were not visible on the aerosol filters, they may have interfered with bubble scavenging and bursting. In contrast to the SAW, aerosol formation in the MIX was considerably more stable within the two monitored days.

4.3 Aerosol composition potentially relates to droplet size and the degradation state of organic matter

The aerosol size spectrum is modulated by jet and film droplets. Jet droplets dominate the aerosol size distribution above 2 µm, whereas film fragments exhibit a peak around 0.2 µm, according to a SSA generation function derived from storm conditions in the Southern Ocean (Deike, 2021). Here, only hydrogels larger than 0.5 µm were assessed. Therewith, film fragments likely dominated the transfer of hydrogels in the smallest size bins (0.5-2.5 µm), while jet droplets controlled the transfer of all larger-sized hydrogels. Jet droplets transport the particulate material from the bubble-scavenged water column (Wang et al., 2015, 2017). Film fragments originate from bursting of the bubble caps at the ocean's interface (Villermaux et al., 2022). During our campaign, SSA hydrogel composition was dependent on the size distribution of SSA and contrasted with the hydrogel repartition of the SSW precursors (Fig. 5). The contribution of proteinaceous material to hydrogels dropped considerably towards larger size bins (2.5-10 µm). Indeed, Wang et al. (2015) observed an even stronger shift in composition as oxygen-containing organics ($C_xH_yO_z$), also equivalent to the molecular formula of carbohydrates, were preferentially enriched in supermicron aerosols. Submicron aerosols, on the other hand, were enriched in aliphatic organics (C_xH_y) such as lipids (Wang et al., 2015) and amino acids (Triesch et al., 2021). While we did not quantify lipids, it is known that proteins (e.g., enzymes) stabilize lipid films in SSA (Luo et al., 2019). Likewise, the organic mass contribution of carbohydrates was reduced in smaller particles (<2.5 µm, 11%) in contrast to larger particles (2.5-10 µm, 27%) in SSA generated during a mesocosm study (Jayarathne et al., 2016). Crocker et al. (2022) reported recently that a different organic matter composition, also of different radiocarbon ages, is transported by sub- versus supermicron particles: Larger jet droplets preferentially transported particulate, fresh organic carbon from a phytoplankton bloom, in contrast to film fragments, which emitted aged

https://doi.org/10.5194/egusphere-2026-1873
Preprint. Discussion started: 10 April 2026

and microbially altered organic carbon, rich in surface-active material and independent of primary biological activity. Bacteria were shown to excrete surface-active material, which stabilizes particulate contaminants such as cells on the bubble film cap despite drainage and evaporation (Poulain & Bourouiba, 2018). Aerosol particles coated in a hydrogel matrix can form during bubble film drainage (Leck & Bigg, 2005; Russell et al., 2010). In summary, different droplet populations are likely formed at different depths involving different mechanisms and the material they transport exhibits different compositions and degradation profiles. We suggest that aerosols do not mirror the size distribution and composition of their precursors in SSW because they form immanently during the process of bubble scavenging and bursting. However, the dynamics of TEP and CSP formation and degradation in the water column and at the air-sea interface may help to understand the size-dependent composition of emitted hydrogels.

4.3.1 Potential biotic and abiotic dynamics influencing SSA precursors

As discussed before, the assembly of large TEP in the surface ocean relies on the size of entangled polymers (Passow, 2000; Verdugo, 2012) and the fraction of acidic sugars involved (Hoagland et al., 1993). Once released by phytoplankton, large polymers and TEP are highly susceptible to, first, photo-degradation (Orellana & Verdugo, 2003; Ortega-Retuerta et al., 2009) and, second, enzymatic breakdown, which is induced by a specialized bacterial consortium and their extracellular enzyme pool (Mari et al., 2017; Reintjes et al., 2019; Sperling et al., 2017). If subjected to irradiation, the aggregation time of TEP are extended, while TEP sizes diminish, and TEP may even completely disperse (Orellana & Verdugo, 2003). UV light exposure also reduces the polyelectrolytic charge of polymers, impeding counterion bonding and reducing hydrogel stability further (Orellana & Verdugo, 2003). A negative correlation of TEP to UV radiation was accordingly found across the equatorial Atlantic Ocean (Zamanillo et al., 2019). Conversely, the bacterial community can considerably enhance aggregation kinetics (Gärdes et al., 2011; Sun et al., 2017), possibly because bacteria benefit from concentrated substrate (Verdugo, 2012). It was shown that diatom-derived exopolymer substances (EPS) released during photosynthesis aggregated only when bacteria were present (Gärdes et al., 2011). Modified by a common marine bacterium that increased the protein-to-carbohydrate ratio, EPS aggregation was enhanced under sunlight irradiation (Song et al., 2015; Sun et al., 2017). It was demonstrated that the addition of proteins (enzymes) supports the enrichment of carbohydrates in supermicron aerosols (Hasenecz et al., 2019). The exposure to solar radiation at the ocean's surface could thus further strengthen the ability of proteins to assemble into heterogeneous polymeric matrices. In line, CSP and amino acids preferably accumulate in the SML and in comparison to carbohydrates (Thornton et al., 2016; Silva et al., 2026). Enriched CSP abundance and area potentially related to heterotrophic bacterial processing and were more independent of wind speed, i.e., bubble scavenging (Engel & Galgani, 2016; Galgani et al., 2016). After a phytoplankton bloom in a microcosm study, extracellular enzymatic activity was enhanced in the SML, and bacterial enzymes (e.g., protease, alkaline phosphatase, and lipases) were effectively emitted and enriched in SSA (Malfatti et al., 2019). These insights may help to understand the compositional shift of size-segregated hydrogels in SSA. While the pool of smaller hydrogels in SSA, which were relatively enriched in CSP (0.5-2.5 µm; Fig. 4a), were likely dominated by film fragments originating from the air-sea interface, the pool of larger, carbohydrate-enriched SSA (2.5-10 µm) were potentially derived

https://doi.org/10.5194/egusphere-2026-1873
Preprint. Discussion started: 10 April 2026

from bubble-scavenging processes in the water column (illustrated in Fig. 7). Therewith, we hypothesize that, particularly at the air–sea interface, bacterial processing favors the accumulation of surface-active, proteinaceous rather than carbohydrate-rich material as TEP may rapidly degrade. This is consistent with both abiotic and biotic degradation processes and with distinct SSA droplet populations that transport TEP and CSP precursors from the water column and the air–sea interface, respectively. Consequently, the observed shift in hydrogel composition, from large carbohydrate-rich to small protein-rich aerosols, can be explained by different formation pathways related to bubble scavenging and bursting, as well as the extent of enzymatic and photochemical degradation.

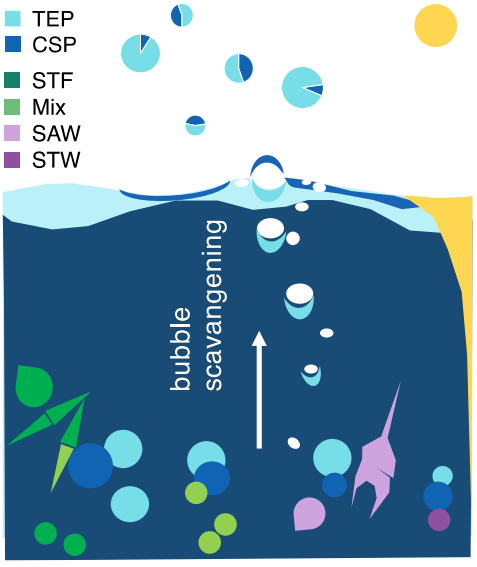

Figure 7 Illustration of hypothesized hydrogel formation and aerosol composition. Transparent exopolymer particles (TEP) are photolabile and preferentially formed in biological active regimes (STF). Nanophytoplankton in the SAW relies on trophic exchange mediated by TEP. Solar radiation and UV light enhances the aggregation process of TEP if bacteria are involved. Bacteria increase the protein-to-carbohydrate ratio while degrading TEP. TEP are primarily assembled and scavenged by bubble plums in the water column, while Coomassie stainable particles (CSP) accumulate and forms also at the air-sea interface. Jet droplets emit TEP from the rear of the bubble, while bubble cap fragments emit microbially altered CSP from the air-sea interface into the atmosphere. Aerosol droplet composition is composed of protein-enriched submicron and carbohydrate-enriched supermicron hydrogels. Abbreviations: Subtropical front (STF), mixed regime (MIX), sub-Antarctic waters (SAW), subtropical waters (STW).

5 Conclusion

With this study, we present the first comprehensive data set of aerosolized hydrogels in characteristic regimes of the Southern hemisphere oceans. We outline (i) the biogeochemical coupling between marine hydrogel dynamics and their atmospheric concentration in SSA, and (ii) link hydrogel composition to potential formation and degradation processes. Hydrogel concentration and enrichment peaked in the subtropical convergence zone (STF) and declined to minima in the open ocean regimes of the subtropical waters, representing the most and the least biologically active regimes in terms of Chl *a* concentration, bacterial abundance, PAA, PCCHO concentration, and TEP abundance and area. However, specific ecosystem variance could not be adequately depicted by total Chl *a* concentration. Hydrogel SSA concentration and enrichment was equal in regimes, which exhibited divergent biogeochemical properties. For instance, the MIX regime, characterized by intermediate Chl *a* concentration, showed lower SSA hydrogel emission than the SAW, which was characterized by lowest Chl *a* concentration. We attribute the enhanced SSA hydrogel concentration and area in the SAW in relation to the MIX to the

https://doi.org/10.5194/egusphere-2026-1873
Preprint. Discussion started: 10 April 2026

occurrence of large carbohydrate polymers, which facilitate aggregation into TEP and supermicron aerosols. We hypothesize that in the SAW severe nutrient limitation promotes mutualistic nanophytoplankton–bacteria interactions that may modulate hydrogel aerosol emissions. The subtropical front (STF) and sub-Antarctic water (SAW) masses are representative of a large area of Southern Ocean biogeochemical conditions (Deppeler & Davidson, 2017). The Southern Ocean possesses a defining role in global weather and climate regulation (Blanco et al., 2023) via biogenic aerosol emissions (McCoy et al., 2015). Based on classical nucleation theory and empirical data, it was recently suggested that 44% of atmospheric ice-nucleating macromolecules in pristine marine air masses of the Southern Ocean are composed of polymeric carbohydrates, which effectively induce ice nucleation between -15 and -20°C (Hartmann et al., 2025). Aside the influence of biogeochemical regimes on hydrogel emission, we further document a shift in the size and composition of hydrogels from precursors to aerosols. We attribute the shift from supermicron carbohydrate-rich to submicron protein-rich aerosols to different formation pathways, and the state of enzymatic and/or photochemical degradation. Enrichment and size-dependency of the SSA composition align well with previous findings, in which hydrogels were not explicitly resolved. We, therefore, agree with the notion that hydrogels may complement a considerable fraction of primary marine aerosols (Facchini et al., 2008; Orellana et al., 2011; Van Pinxteren et al., 2022; Hartmann et al., 2025). As the data availability is limited and the variability is large, the emerging pattern of hydrogels in SSA described here should be interpreted with caution. Future studies should explore whether hydrogel aggregation, their emission, and enzyme activity are mutually dependent as hydrogels and enzymes likely represent excellent cloud condensation and ice nuclei (Alsante et al., 2023; Cascajo-Castresana et al., 2020; Ovadnevaite et al., 2011; Wilson et al., 2015).

Appendix

Table A1 Surface seawater (SSW) station overview including time of sampling and regime. Abbreviations: morning (am), afternoon (pm), subtropical front (STF), sub-Antarctic waters (SAW), subtropical waters (STW), and the mixed regime with Cook-Strait influenced waters (MIX).

Station-ID	Sampling	Date	Longitude	Latitude	Time of the day	Regime
		[dd.mm.yy]	[deg]	[deg]	*cat.*	*cat.*
UW02	underway	17.03.20	174,333149	-43,245861	am	STF
UW03	underway	17.03.20	174,285049	-43,627523	pm	STF
UW04_1	working boat	18.03.20	173,991589	-44,398507	am	STF
UW05	underway	18.03.20	174,425712	-44,506587	pm	STF
UW06_1	working boat	19.03.20	175,345191	-44,720536	am	STF
UW07	underway	19.03.20	174,957502	-44,649301	pm	STF
UW09	underway	20.03.20	175,113783	-44,674284	am	STF
UW10	underway	20.03.20	175,170186	-45,005539	pm	STF
UW12_1	working boat	21.03.20	175,152293	-45,819486	am	SAW
UW13	underway	21.03.20	175,601954	-45,778226	pm	SAW
UW15	underway	22.03.20	177,230524	-45,848717	am	SAW
UW16	underway	22.03.20	177,083713	-45,828553	pm	SAW
UW17_1	working boat	23.03.20	177,083758	-46,000588	am	SAW
UW18	underway	23.03.20	176,839173	-45,433426	pm	SAW
UW20	underway	24.03.20	176,737372	-42,970412	am	STW
UW21	underway	24.03.20	177,092545	-42,518821	pm	STW
UW23	underway	25.03.20	175,582664	-42,399331	am	MIX
UW23_1	working boat	25.03.20	175,502197	-42,567109	pm	MIX
UW24_1	working boat	26.03.20	174,633941	-42,751039	am	MIX
UW24_2	working boat	26.03.20	174,211285	-42,698915	pm	MIX

https://doi.org/10.5194/egusphere-2026-1873
Preprint. Discussion started: 10 April 2026

Table A2 Station overview for sea spray aerosol filters (SSA) including the duration of sample collection and regimes. Abbreviations: Natrium (Na), Sea spray aerosols (SSA), subtropical front (STF), Sub-Antarctic waters (SAW), subtropical waters (STW), and the Mixed regime with Cook-Strait influenced waters (Mix).

Station-ID	Sampling	Date	Filtration time	Air Volume	Na in SSA	Regime
		[dd.mm.yy]	[h]	[m^3]	[µg m^3]	*cat.*
UW07	underway	19.03.20	24	4,17	0,019	STF
UW10	underway	20.03.20	22	1,45	0,023	STF
UW13	underway	21.03.20	22	4,09	0,050	SAW
UW16	underway	22.03.20	22	2,05	0,024	SAW
UW18	underway	23.03.20	23.5	2,19	0,025	SAW
UW21	underway	24.03.20	22.5	3,98	0,052	STW
UW23_1	underway	25.03.20	20.5	1,85	n/a	MIX
UW24_2	underway	26.03.20	18.5	3,33	n/a	MIX

Table A4 Overview of the mean concentration and standard deviation of bulk parameters grouped in the categories time of day and regimes (sampling period between 17.06.2020 and 26.03.2020 for surface seawater). SSW samples influenced by soot are excluded. SSW CSP area [%] includes only samples generated between 19.03. to 26.03.2020 in equivalence to the sea spray aerosol (SSA) collection (Hydrogels, CSP in SSA). To approximate the CSP area in SSA, an alternative staining method was applied (*, Supplementary Information). Only significant *p*-values are presented, *p*-values for which this was not the case have been replaced by n/a. In the case of SSA samples, statistics could not be assessed due to data scarcity, which is also indicated by n/a. Additional statistical information for the parameters assessed in sea water are represented in Table A2. Abbreviations: total organic carbon (TOC), total organic nitrogen (TON), particulate carbohydrates (PCCHO), particulate amino acids (PAA), dissolved combined carbohydrates (DCCHO), dissolved amino acids (DAA), afternoon (pm), morning (am), subtropical front (STF), mixed regimes (MIX), sub-Antarctic waters (SAW), subtropical waters (STW), not applicable (n/a).

Factor	**Time of the day**			**Regime**				
Category	pm	am	art ANOVA	STF	MIX	SAW	STW	art ANOVA
Data format	[mean ± SD]	[mean ± SD]	*p-value <0.05*	[mean ± SD]	[mean ± SD]	[mean ± SD]	[mean ± SD]	*p-value <0.05*
TEP abundance [× 10^6 L^{-1}]	41 ± 19	30 ± 11	n/a	45 ± 15	34 ± 8	22 ± 7	19 ± 1	0.0227
TEP slope [δ]	-2.49 ± 0.20	-2.46 ± 0.16	n/a	-2.37 ± 0.15	-2.71 ± 0.07	-2.47 ± 0.04	-2.39 ± 0.08	0.0159
CSP abundance [× 10^6 L^{-1}]	40 ± 10	37 ± 12	n/a	41 ± 11	45 ± 11	29 ± 5	31 ± 11	n/a
CSP slope [δ]	-2.42 ± 0.24	-2.50 ± 0.16	n/a	-2.35 ± 0.18	-2.68 ± 0.15	-2.53 ± 0.06	-2.36 ± 0.16	n/a
TEP area [mm^2 L^{-1}]	186 ± 87	160 ± 87	n/a	248 ± 67	102 ± 31	120 ± 35	109 ± 33	0.0080
CSP area [mm^2 L^{-1}]	291 ± 129	214 ± 74	0.0387	333 ± 103	192 ± 55	158 ± 14	203 ± 33	0.0001
CSP area [%]	61 ± 5	59 ± 8	n/a	57 ± 7	65 ± 3	58 ± 8	65 ± 3	n/a
Hydrogels in SSA [× 10^5 m^{-3}]	n/a	n/a	n/a	0.91 ± 0.72	0.28 ± 0.03	0.43 ± 0.15	0.18	n/a
Hydrogels in SSA, slope [δ]	n/a	n/a	n/a	-2.07 ± 0.13	-1.78 ± 0.03	-2.07 ± 0.22	-1.87	n/a
Hydrogels in SSA [mm^2 m^{-3}]	n/a	n/a	n/a	2.45 ± 2.16	1.05 ± 0.00	1.13 ± 0.87	0.52	n/a
CSP area in SSA* [%]	n/a	n/a	n/a	13 ± 3	5 ± 2	10 ± 6	11	n/a
TOC [µM]	81.1 ± 10.9	76.7 ±10.4	n/a	88.7 ±10.4	74.0 ±2.3	70.4 ±2.4	74.9 ±2.0	0.0001
TON [µM]	7.1 ± 2.1	6.7 ± 1.3	n/a	8.4 ± 1.4	6.4 ± 0.3	5.4 ± 1.4	6.9 ± 0.2	0.0001
PCCHO [nM]	579 ± 587	236 ± 312	0.0279	798 ± 574	224 ± 244	123 ± 47	72 ± 22	0.0002
PAA [nM]	537 ± 299	523 ± 443	n/a	854 ± 361	430 ± 202	281 ± 90	183 ± 31	n/a

https://doi.org/10.5194/egusphere-2026-1873
Preprint. Discussion started: 10 April 2026

DCCHO [nM]	786 ± 326	570 ± 200	0.0296	903 ± 323	498 ± 48	500 ± 59	676 ± 264	0.0004
DAA [nM]	392 ± 141	305 ± 52	0.0371	386 ± 168	371 ± 49	303 ± 31	293 ± 36	n/a
Bacteria [× 10^6 cells mL^{-1}]	2.67 ± 0.92	2.52 ± 0.65	n/a	3.02 ± 0.46	3.00 ± 0.98	1.90 ± 0.50	1.87 ± 0.43	0.0200
Synechococcus [× 10^3 cells mL^{-1}]	62 ± 32	83 ± 45	n/a	74 ± 48	88 ± 48	57 ± 77	59 ± 33	n/a
Picophytoplankton [× 10^3 cells mL^{-1}]	12.0 ± 4.6	16.4 ± 4.8	n/a	13.0 ± 5.9	15.8 ± 5.4	14.7 ± 3.2	12.6 ± 6.9	n/a
Nanophytoplankton [× 10^3 cells mL^{-1}]	1.43 ± 0.80	1.77 ± 0.84	0.0354	2.31 ± 0.45	0.81 ± 0.38	1.26 ± 0.62	0.84 ± 0.05	0.0008
total Chlorophyll *a* [mg m^{-3}]	1.12 ± 0.90	1.15 ± 1.02	n/a	2.06 ± 0.79	0.82 ± 0.24	0.36 ± 0.05	0.39 ± 0.13	0.0001
Chlorophyll *a* 0.2-2 µm [mg m^{-3}]	0.28 ± 0.16	0.34 ± 0.16	n/a	0.42 ± 0.15	0.39 ± 0.07	0.15 ± 0.06	0.18 ± 0.03	0.0011
Chlorophyll *a* 2-20 µm [mg m^{-3}]	0.35 ± 0.28	0.46 ± 0.47	n/a	0.73 ± 0.42	0.26 ± 0.13	0.13 ± 0.04	0.18 ± 0.07	0.0015
Chlorophyll *a* >20 µm [mg m^{-3}]	0.49 ± 0.54	0.36 ± 0.43	n/a	0.91 ± 0.39	0.17 ± 0.16	0.08 ± 0.04	0.02 ± 0.03	0.0005

Table A4 Complementary F-statistics as calculated for the times of the day and regimes for biogeochemical parameters in sea water. The table refers to the concentrations presented in Table A3. Bold numbers indicate significance and the asterisks mark the level of significance (∗*p*-value<0.05; ∗∗*p*-value<0.01; ∗∗∗*p*-value<0.001).

Time and Regime	Aligned rank transformation ANOVA [*F* value]		
	TAN2003 (N=20, DFs 15)		
Category	Time	Regime	Interaction
TEP abundance [× 10^6 L^{-1}]	3.4	**4.9***	0.5
CSP abundance [× 10^6 L^{-1}]	0.5	2.9	0.9
TEP area [mm^2 L^{-1}]	1.4	**7.0****	0.7
CSP area [mm^2 L^{-1}]	**5.7***	**13.0*****	0.1
TOC [µM]	3.6	**23.2*****	0.6
TON [µM]	0.5	**25.4*****	0.7
PCCHO [nM]	**6.3***	**15.6*****	1.9
PAA [nM]	0.1	**10.7****	1.4
DCCHO [nM]	**6.1***	**13.4*****	2.6
DAA [nM]	**5.5***	1.7	2.2

https://doi.org/10.5194/egusphere-2026-1873
Preprint. Discussion started: 10 April 2026

https://doi.org/10.5194/egusphere-2026-1873
Preprint. Discussion started: 10 April 2026

560

Bacteria [× 10^6 cells mL^{-1}]	0.1	**5.0***	0.3	
Synechococcus spp. [×10^3 cells mL^{-1}]	0.5	0.1	0.2	
Picophytoplankton [× 10^3 cells mL^{-1}]	1.3	0.2	0.2	
Nanophytoplankton [× 10^3 cells mL^{-1}]	**6.1***	**14.8*****	1.0	
Chlorophyll *a* 0.2-2 µm [mg m^{-3}]	2.0	**10.7****	0.2	
Chlorophyll *a* 2-20 µm [mg m^{-3}]	4.0	**9.8****	1.6	
Chlorophyll *a* >20 µm [mg m^{-3}]	2.5	**12.9*****	2.2	

https://doi.org/10.5194/egusphere-2026-1873
Preprint. Discussion started: 10 April 2026

Author contributions

TB and KSe designed the study. TB performed sampling of hydrogels and further biogeochemical parameters in seawater, KSe performed sampling of aerosolized hydrogels, KSa collected samples for the phytoplankton community composition with the help of technicians and students. LS and BP developed the approach for simultaneous staining of carbohydrate- and protein-rich hydrogels. All parameters were measured at the GEOMAR or NIWA laboratory. TB analyzed the data with help from LS (composition of SSA hydrogels). TB and AE wrote the manuscript. TB, KSe, BP, AE edited and proof-read the manuscript.

Data availability

Biogeochemically data are published in an open access repository and are available online (Barthelmeß et al., 2025; https://doi.pangaea.de/10.1594/PANGAEA.974276). SSW and SSA hydrogel data will be made available in the same repository upon publication.

Competing interests

The authors have no competing interests to declare.

Disclaimer

Copernicus Publications adds a standard disclaimer: "Copernicus Publications remains neutral with regard to jurisdictional claims made in the text, published maps, institutional affiliations, or any other geographical representation in this paper. While Copernicus Publications makes every effort to include appropriate place names, the final responsibility lies with the authors. Views expressed in the text are those of the authors and do not necessarily reflect the views of the publisher."
Please feel free to add disclaimer text at your choice, if applicable.

Acknowledgements

We are very thankful for the support of our chief scientist Cliff S. Law, the crew of the RV Tangaroa, and all the scientists, students, and technicians who helped to collect and measure the samples, in particular Jonathan Trueblood, Wayne Dillon, and Antonia Cristi, Stacy Deppeler on board, Jon Roa, Sandra Golde, Ruth Flerus, and Tania Klüver at GEOMAR Helmholtz Centre for Ocean Research Kiel. This paper contributes to the science plan of the Surface Ocean-Lower Atmosphere Study (SOLAS), which is partially supported by the U.S. National Science Foundation (Grant OCE-1840868) via the Scientific Committee on Oceanic Research (SCOR).

https://doi.org/10.5194/egusphere-2026-1873
Preprint. Discussion started: 10 April 2026

Financial support

This research was funded by the European Research Council (ERC) under the Horizon 2020 research and innovation program (Sea2Cloud grant agreement number 771369 and grant agreement number 101002728) and was supported by NIWA SSIF funding. The support of the German Academic Exchange Service (DAAD) is greatly appreciated (57438025).

Review statement

The review statement will be added by Copernicus Publications listing the handling editor as well as all contributing referees according to their status anonymous or identified.

References

Alldredge, A. L., Passow, U., & Logan, B. E. (1993). The abundance and significance of a class of large, transparent organic particles in the ocean. *Deep Sea Research Part I: Oceanographic Research Papers*, *40*(6), 1131–1140. https://doi.org/https://doi.org/10.1016/0967-0637(93)90129-Q

Aller, J. Y., Radway, J. A. C., Kilthau, W. P., Bothe, D. W., Wilson, T. W., Vaillancourt, R. D., Quinn, P. K., Coffman, D. J., Murray, B. J., & Knopf, D. A. (2017). Size-resolved characterization of the polysaccharidic and proteinaceous components of sea spray aerosol. *Atmospheric Environment*, *154*(February), 331–347. https://doi.org/10.1016/j.atmosenv.2017.01.053

Alsante, A. N., Thornton, D. C. O., & Brooks, S. D. (2023). Ice nucleation catalyzed by the photosynthesis enzyme RuBisCO and other abundant biomolecules. *Communications Earth and Environment*, *4*(1), 1–9. https://doi.org/10.1038/s43247-023-00707-7

Amin, S. A., Green, D. H., Hart, M. C., Küpper, F. C., Sunda, W. G., & Carrano, C. J. (2009). Photolysis of iron-siderophore chelates promotes bacterial-algal mutualism. *Proceedings of the National Academy of Sciences of the United States of America*, *106*(40), 17071–17076. https://doi.org/10.1073/pnas.0905512106

Amin, S. A., Hmelo, L. R., Van Tol, H. M., Durham, B. P., Carlson, L. T., Heal, K. R., Morales, R. L., Berthiaume, C. T., Parker, M. S., Djunaedi, B., Ingalls, A. E., Parsek, M. R., Moran, M. A., & Armbrust, E. V. (2015). Interaction and signalling between a cosmopolitan phytoplankton and associated bacteria. *Nature*, *522*(7554), 98–101. https://doi.org/10.1038/nature14488

Barthelmeß, T., Cristi, A., Deppeler S., Safi, K., Sellegri, K., Law, C. S. and Engel, A. (2025). Pronounced Diel Cycling of Dissolved Carbohydrates and Amino Acids in the Surface Ocean and across Diverse Regimes. *Environmental Science and Technology*, *59, 1,* 419–429. https://pubs.acs.org/doi/10.1021/acs.est.4c00491.

https://doi.org/10.5194/egusphere-2026-1873
Preprint. Discussion started: 10 April 2026

Barthelmeß, T., Cristi, A., Deppeler S., Safi, K., Sellegri, K., Law, C. S. and Engel, A. (2025). Diel dissolved organic matter cycling and phytoplankton abundance in four trophic regimes of the South Pacific Ocean [dataset bundled publication]. *PANGAEA*. https://doi.pangaea.de/10.1594/PANGAEA.974276.

Behrenfeld, M. J., Boss, E., Siegel, D. A., & Shea, D. M. (2005). Carbon-based ocean productivity and phytoplankton physiology from space. *Global Biogeochemical Cycles*, *19*(1), 1–14. https://doi.org/10.1029/2004GB002299

Bell, W., & Mitchell, R. (1972). Chemotactic and Growth Responses of Marine Bacteria To Algal Extracellular Products. In *The Biological Bulletin* (Vol. 143, Issue 2, pp. 265–277). Woods Hole, Mass Marine Biological Laboratory. https://doi.org/10.2307/1540052

Blanchard, D. C. (1989). The ejection of drops from the sea and their enrichment with bacteria and other materials: A review. *Estuaries*, *12*(3), 127–137. https://doi.org/10.2307/1351816

Blanco, J. E., Caballero, R., Datseris, G., Stevens, B., Bony, S., Hadas, O., & Kaspi, Y. (2023). A Cloud-Controlling Factor Perspective on the Hemispheric Asymmetry of Extratropical Cloud Albedo. *Journal of Climate*, *36*(6), 1793–1804. https://doi.org/10.1175/JCLI-D-22-0410.1

Borchard, C., & Engel, A. (2015). Size-fractionated dissolved primary production and carbohydrate composition of the coccolithophore Emiliania huxleyi. *Biogeosciences*, *12*(4), 1271–1284. https://doi.org/10.5194/bg-12-1271-2015

Brooks, S. D., & Thornton, D. C. O. (2018). Marine aerosols and clouds. In *Annual Review of Marine Science* (Vol. 10, pp. 289–313). https://doi.org/10.1146/annurev-marine-121916-063148

Burrows, S. M., Ogunro, O., Frossard, A. A., Russell, L. M., Rasch, P. J., & Elliott, S. M. (2014). A physically based framework for modeling the organic fractionation of sea spray aerosol from bubble film Langmuir equilibria. *Atmospheric Chemistry and Physics*, *14*(24), 13601–13629. https://doi.org/10.5194/acp-14-13601-2014

Cascajo-Castresana, M., David, R. O., Iriarte-Alonso, M. A., Bittner, A. M., & Marcolli, C. (2020). Protein aggregates nucleate ice: The example of apoferritin. *Atmospheric Chemistry and Physics*, *20*(6), 3291–3315. https://doi.org/10.5194/acp-20-3291-2020

Chien, C. Te, Pahlow, M., Schartau, M., Li, N., & Oschlies, A. (2023). Effects of phytoplankton physiology on global ocean biogeochemistry and climate. *Science Advances*, *9*(30), 1–10. https://doi.org/10.1126/sciadv.adg1725

Cisternas-Novoa, C., Lee, C., & Engel, A. (2015). Transparent exopolymer particles (TEP) and Coomassie stainable particles (CSP): Differences between their origin and vertical distributions in the ocean. *Marine Chemistry*, *175*, 56–71. https://doi.org/10.1016/j.marchem.2015.03.009

Crocker, D. R., Kaluarachchi, C. P., Cao, R., Dinasquet, J., Franklin, E. B., Morris, C. K., Amiri, S., Petras, D., Nguyen, T., Torres, R. R., Martz, T. R., Malfatti, F., Goldstein, A. H., Tivanski, A. V., Prather, K. A., & Thiemens, M. H. (2022). Isotopic Insights into Organic Composition Differences between Supermicron and Submicron Sea Spray Aerosol. *Environmental Science and Technology*, *56*(14), 9947–9958. https://doi.org/10.1021/acs.est.2c02154

https://doi.org/10.5194/egusphere-2026-1873
Preprint. Discussion started: 10 April 2026

Davis, J., & Benner, R. (2007). Quantitative estimates of labile and semi-labile dissolved organic carbon in the western Arctic Ocean: A molecular approach. *Limnology and Oceanography*, *52*(6), 2434–2444. https://doi.org/10.4319/lo.2007.52.6.2434

Davis, J., Kaiser, K., & Benner, R. (2009). Amino acid and amino sugar yields and compositions as indicators of dissolved organic matter diagenesis. *Organic Geochemistry*, *40*(3), 343–352. https://doi.org/10.1016/j.orggeochem.2008.12.003

Deike, L. (2021). Mass Transfer at the Ocean-Atmosphere Interface: The Role of Wave Breaking, Droplets, and Bubbles. *Annual Review of Fluid Mechanics*, *54*, 191–224. https://doi.org/10.1146/annurev-fluid-030121-014132

Deppeler, S. L., & Davidson, A. T. (2017). Southern Ocean phytoplankton in a changing climate. *Frontiers in Marine Science*, *4*(FEB). https://doi.org/10.3389/fmars.2017.00040

Dreshchinskii, A. und Engel, A. (2017). Seasonal variations of the sea surface microlayer at the Boknis Eck Times Series Station (Baltic Sea). *Journal of Plankton Research*, 39 (6). pp. 943-961. https://doi.org/10.1093/plankt/fbx055.

Dukhin, S. S., Kovalchuk, V. I., Gochev, G. G., Lotfi, M., Krzan, M., Malysa, K., & Miller, R. (2015). Dynamics of Rear Stagnant Cap formation at the surface of spherical bubbles rising in surfactant solutions at large Reynolds numbers under conditions of small Marangoni number and slow sorption kinetics. *Advances in Colloid and Interface Science*, *222*(2013), 260–274. https://doi.org/10.1016/j.cis.2014.10.002

Durham, B. P., Sharma, S., Luo, H., Smith, C. B., Amin, S. A., Bender, S. J., Dearth, S. P., Van Mooy, B. A. S., Campagna, S. R., Kujawinski, E. B., Armbrust, E. V., & Moran, M. A. (2015). Cryptic carbon and sulfur cycling between surface ocean plankton. *Proceedings of the National Academy of Sciences of the United States of America*, *112*(2), 453–457. https://doi.org/10.1073/pnas.1413137112

Engel, A. (2009). *Determination of Marine Gel Particles , Practical guidelines for the analysis of seawater* (O. Wurl, B. Raton, & [u.a.] (eds.)). CRC Press.

Engel, A., Delille, B., Jacquet, S., Riebesell, U., Rochelle-Newall, E., Terbrüggen, A., & Zondervan, I. (2004). Transparent exopolymer particles and dissolved organic carbon production by Emiliania huxleyi exposed to different CO2 concentrations: A mesocosm experiment. *Aquatic Microbial Ecology*, *34*(1), 93–104. https://doi.org/10.3354/ame034093

Engel, A., Endres, S., Galgani, L., & Schartau, M. (2020). Marvelous Marine Microgels: On the Distribution and Impact of Gel-Like Particles in the Oceanic Water-Column. *Frontiers in Marine Science*, *7*(June), 1–15. https://doi.org/10.3389/fmars.2020.00405

Engel, A., & Galgani, L. (2016). The organic sea-surface microlayer in the upwelling region off the coast of Peru and potential implications for air-sea exchange processes. *Biogeosciences*, *13*(4), 989–1007. https://doi.org/10.5194/bg-13-989-2016

Engel, A., Piontek, J., Metfies, K., Endres, S., Sprong, P., Peeken, I., Gäbler-Schwarz, S., & Nöthig, E. M. (2017). Inter-annual variability of transparent exopolymer particles in the Arctic Ocean reveals high sensitivity to ecosystem changes. *Scientific Reports*, *7*(1), 1–9. https://doi.org/10.1038/s41598-017-04106-9

https://doi.org/10.5194/egusphere-2026-1873
Preprint. Discussion started: 10 April 2026

Facchini, M. C., Rinaldi, M., Decesari, S., Carbone, C., Finessi, E., Mircea, M., Fuzzi, S., Ceburnis, D., Flanagan, R., Nilsson, E. D., de Leeuw, G., Martino, M., Woeltjen, J., & O'Dowd, C. D. (2008). Primary submicron marine aerosol dominated by insoluble organic colloids and aggregates. *Geophysical Research Letters*, *35*(17), 1–5. https://doi.org/10.1029/2008GL034210

Fan, S. M., Horowitz, L. W., Levy, H., & Moxim, W. J. (2004). Impact of air pollution on wet deposition of mineral dust aerosols. *Geophysical Research Letters*, *31*(2), 2–5. https://doi.org/10.1029/2003GL018501

Fuentes, E., Coe, H., Green, D., De Leeuw, G., & McFiggans, G. (2010). Laboratory-generated primary marine aerosol via bubble-bursting and atomization. *Atmospheric Measurement Techniques*, *3*(1), 141–162. https://doi.org/10.5194/amt-3-141-2010

Galgani, L., Piontek, J., & Engel, A. (2016). Biopolymers form a gelatinous microlayer at the air-sea interface when Arctic sea ice melts. *Scientific Reports*, *6*(July), 1–10. https://doi.org/10.1038/srep29465

Gärdes, A., Iversen, M. H., Grossart, H. P., Passow, U., & Ullrich, M. S. (2011). Diatom-associated bacteria are required for aggregation of Thalassiosira weissflogii. *ISME Journal*, *5*(3), 436–445. https://doi.org/10.1038/ismej.2010.145

Halsey, K. H., & Jones, B. M. (2015). Phytoplankton Strategies for Photosynthetic Energy Allocation. *Annual Review of Marine Science*, *7*(1), 265–297. https://doi.org/10.1146/annurev-marine-010814-015813

Hansell, D. A., Carlson, C. A., Repeta, D. J., & Schlitzer, R. (2009). Dissolved organic matter in the ocean a controversy stimulates new insights. *Oceanography*, *22*(SPL.ISS. 4), 202–211. https://doi.org/10.5670/oceanog.2009.109

Hartmann, S., Schrödner, R., Hassett, B.T., Hartmann, M., van Pinxteren, M., Fomba, K.W., Stratmann, F., Herrmann, H., Pöhlker, M., and Zeppendeld, S. (2025). Polysaccharides–Important Constitutes of Ice-Nucleating Particles of Marine Origin. *Environmental Science and Technology, 59*, 5098-5108. https://doi.org/10.1021/acs.est.4c08014.

Hasenecz, E. S., Kaluarachchi, C. P., Lee, H. D., Tivanski, A. V., & Stone, E. A. (2019). Saccharide Transfer to Sea Spray Aerosol Enhanced by Surface Activity, Calcium, and Protein Interactions. *ACS Earth and Space Chemistry*, *3*(11), 2539–2548. https://doi.org/10.1021/acsearthspacechem.9b00197

Hassler, C. S., Schoemann, V., Nichols, C. M., Butler, E. C. V., & Boyd, P. W. (2011). Saccharides enhance iron bioavailability to southern ocean phytoplankton. *Proceedings of the National Academy of Sciences of the United States of America*, *108*(3), 1076–1081. https://doi.org/10.1073/pnas.1010963108

Hoagland, K., Rosowski, J., Gretz, M., & Roemer, S. (1993). Diatom extracellular polymeric substances: Function, fine structure, chemistry and physiology. *Journal of Phycology*, *29*, 537–566. http://www.nber.org/papers/w16019

Jayarathne, T., Sultana, C. M., Lee, C., Malfatti, F., Cox, J. L., Pendergraft, M. A., Moore, K. A., Azam, F., Tivanski, A. V., Cappa, C. D., Bertram, T. H., Grassian, V. H., Prather, K. A., & Stone, E. A. (2016). Enrichment of Saccharides and Divalent Cations in Sea Spray Aerosol during Two Phytoplankton Blooms. *Environmental Science and Technology*, *50*(21), 11511–11520. https://doi.org/10.1021/acs.est.6b02988

https://doi.org/10.5194/egusphere-2026-1873
Preprint. Discussion started: 10 April 2026

Jenkinson, I. R., Seuront, L., Ding, H., & Elias, F. (2018). Biological modification of mechanical properties of the sea surface microlayer, influencing waves, ripples, foam and air-sea fluxes. *Elementa: Science of the Anthropocene*, *6*, 26. https://doi.org/10.1525/elementa.283

Kuznetsova, M., Lee, C., & Aller, J. (2005). Characterization of the proteinaceous matter in marine aerosols. *Marine Chemistry*, *96*(3–4), 359–377. https://doi.org/10.1016/j.marchem.2005.03.007

Law, C. S., Smith, M. J., Harvey, M. J., Bell, T. G., Cravigan, L. T., Elliott, F. C., Lawson, S. J., Lizotte, M., Marriner, A., McGregor, J., Ristovski, Z., Safi, K. A., Saltzman, E. S., Vaattovaara, P., & Walker, C. F. (2017). Overview and preliminary results of the Surface Ocean Aerosol Production (SOAP) campaign. *Atmospheric Chemistry and Physics*. https://doi.org/10.5194/acp-17-13645-2017

Leck, C., & Bigg, E. K. (2005). Biogenic particles in the surface microlayer and overlaying atmosphere in the central Arctic Ocean during summer. *Tellus B: Chemical and Physical Meteorology*, *57*(4), 305–316. https://doi.org/10.3402/tellusb.v57i4.16546

Lhuissier, H., & Villermaux, E. (2012). Bursting bubble aerosols. *Journal of Fluid Mechanics*, *696*, 5–44. https://doi.org/10.1017/jfm.2011.418

Long, M. S., Keene, W. C., Quinn, P. K., & Bates, T. S. (2014). Light-enhanced primary marine aerosol production from biologically productive seawater. *Geophysical Prospecting*, *April*, 6413–6419. https://doi.org/10.1002/2014GL061184.Received

Long, R. A., & Azam, F. (1996). Abundant protein-containing particles in the sea. *Aquatic Microbial Ecology*, *10*(3), 213–221. https://doi.org/10.3354/ame010213

Luo, M., Dommer, A. C., Schiffer, J. M., Rez, D. J., Mitchell, A. R., Amaro, R. E., & Grassian, V. H. (2019). Surfactant Charge Modulates Structure and Stability of Lipase-Embedded Monolayers at Marine-Relevant Aerosol Surfaces. *Langmuir*, *35*(27), 9050–9060. https://doi.org/10.1021/acs.langmuir.9b00689

Malfatti, F., Lee, C., Tinta, T., Pendergraft, M. A., Celussi, M., Zhou, Y., Sultana, C. M., Rotter, A., Axson, J. L., Collins, D. B., Santander, M. V., Anides Morales, A. L., Aluwihare, L. I., Riemer, N., Grassian, V. H., Azam, F., & Prather, K. A. (2019). Detection of Active Microbial Enzymes in Nascent Sea Spray Aerosol: Implications for Atmospheric Chemistry and Climate. *Environmental Science and Technology Letters*, *6*(3), 171–177. https://doi.org/10.1021/acs.estlett.8b00699

Mari, X., Lefèvre, J., Torréton, J.-P., Weinbauer, M. G., & Legendre, L. (2014). Global biogeochemical cycles. *Global Biogeochemical Cycles*, *28*, 927–949. https://doi.org/10.1002/2014GB004878.Received

Mari, X., Passow, U., Migon, C., Burd, A. B., & Legendre, L. (2017). Transparent exopolymer particles: Effects on carbon cycling in the ocean. *Progress in Oceanography*, *151*, 13–37. https://doi.org/10.1016/j.pocean.2016.11.002

McCluskey, C. S., Hill, T. C. J., Malfatti, F., Sultana, C. M., Lee, C., Santander, M. V., Beall, C. M., Moore, K. A., Cornwell, G. C., Collins, D. B., Prather, K. A., Jayarathne, T., Stone, E. A., Azam, F., Kreidenweis, S. M., & DeMott, P. J. (2017). A dynamic link between ice nucleating particles released in nascent sea spray aerosol and oceanic biological activity

https://doi.org/10.5194/egusphere-2026-1873
Preprint. Discussion started: 10 April 2026

during two mesocosm experiments. *Journal of the Atmospheric Sciences*, *74*(1), 151–166. https://doi.org/10.1175/JAS-D-16-0087.1

McCoy, D. T., Burrows, S. M., Wood, R., Grosvenor, D. P., Elliott, S. M., Ma, P. L., Rasch, P. J., & Hartmann, D. L. (2015). Natural aerosols explain seasonal and spatial patterns of Southern Ocean cloud albedo. *Science Advances*, *1*(6). https://doi.org/10.1126/sciadv.1500157

Mitts, B. A., Wang, X., Lucero, D. D., Beall, C. M., Deane, G. B., DeMott, P. J., & Prather, K. A. (2021). Importance of Supermicron Ice Nucleating Particles in Nascent Sea Spray. *Geophysical Research Letters*, *48*(3), 1–10. https://doi.org/10.1029/2020GL089633

Moore, C. M., Mills, M. M., Arrigo, K. R., Berman-Frank, I., Bopp, L., Boyd, P. W., Galbraith, E. D., Geider, R. J., Guieu, C., Jaccard, S. L., Jickells, T. D., La Roche, J., Lenton, T. M., Mahowald, N. M., Marañón, E., Marinov, I., Moore, J. K., Nakatsuka, T., Oschlies, A., … Ulloa, O. (2013). Processes and patterns of oceanic nutrient limitation. *Nature Geoscience*, *6*(9), 701–710. https://doi.org/10.1038/ngeo1765

Moran, M. A., Ferrer-González, F. X., Fu, H., Nowinski, B., Olofsson, M., Powers, M. A., Schreier, J. E., Schroer, W. F., Smith, C. B., & Uchimiya, M. (2022). The Ocean's labile DOC supply chain. In *Limnology and Oceanography* (Vol. 67, Issue 5, pp. 1007–1021). https://doi.org/10.1002/lno.12053

Murphy, R. J., Pinkerton, M. H., Richardson, K. M., Bradford-Grieve, J. M., & Boyd, P. W. (2001). Phytoplankton distributions around New Zealand derived from SeaWiFS remotely-sensed ocean colour data. *New Zealand Journal of Marine and Freshwater Research*, *35*(2), 343–362. https://doi.org/10.1080/00288330.2001.9517005

Myklestad, S. M. (1995). Release of extracellular products by phytoplankton with special emphasis on polysaccharides. *Science of the Total Environment*, *165*(1–3), 155–164. https://doi.org/10.1016/0048-9697(95)04549-G

O'dowd, C., Ceburnis, D., Ovadnevaite, J., Bialek, J., Stengel, D. B., Zacharias, M., Nitschke, U., Connan, S., Rinaldi, M., Fuzzi, S., Decesari, S., Cristina Facchini, M., Marullo, S., Santoleri, R., Dell'anno, A., Corinaldesi, C., Tangherlini, M., & Danovaro, R. (2015). Connecting marine productivity to sea-spray via nanoscale biological processes: Phytoplankton Dance or Death Disco? *Scientific Reports*, *5*(May), 1–11. https://doi.org/10.1038/srep14883

O'Dowd, C. D., Facchini, M. C., Cavalli, F., Ceburnis, D., Mircea, M., Decesari, S., Fuzzi, S., Young, J. Y., & Putaud, J. P. (2004). Biogenically driven organic contribution to marine aerosol. *Nature*, *431*(7009), 676–680. https://doi.org/10.1038/nature02959

Orellana, M. V., & Verdugo, P. (2003). Ultraviolet radiation blocks the organic carbon exchange between the dissolved phase and the gel phase in the ocean. *Limnology and Oceanography*, *48*(4), 1618–1623. https://doi.org/10.4319/lo.2003.48.4.1618

Orellana, M. V, Matrai, P. A., Leck, C., Rauschenberg, C. D., Lee, A. M., & Coz, E. (2011). Marine microgels as a source of cloud condensation nuclei in the high arctic. *Proceedings of the National Academy of Sciences of the United States of America*, *108*(33), 13612–13617. https://doi.org/10.1073/pnas.1102457108

https://doi.org/10.5194/egusphere-2026-1873
Preprint. Discussion started: 10 April 2026

Ortega-Retuerta, E., Passow, U., Duarte, C. M., & Reche, I. (2009). Effects of ultraviolet B radiation on (not so) transparent exopolymer particles. *Biogeosciences*, *6*(12), 3071–3080. https://doi.org/10.5194/bg-6-3071-2009

Ovadnevaite, J., Ceburnis, D., Martucci, G., Bialek, J., Monahan, C., Rinaldi, M., Facchini, M. C., Berresheim, H., Worsnop, D. R., & O'Dowd, C. (2011). Primary marine organic aerosol: A dichotomy of low hygroscopicity and high CCN activity. *Geophysical Research Letters*, *38*(21), 1–5. https://doi.org/10.1029/2011GL048869

Passow, U. (2000). Formation of transparent exopolymer particles, TEP, from dissolved precursor material. *Mar. Ecol. Prog. Ser.* 192, 1-11. https://doi.org/10.3354/meps192001

van Pinxteren, M., Robinson, T.-B., Zeppenfeld, S., Gong, X., Bahlmann, E., Fomba, K.W., Triesch, N., Stratmann, F., Wurl, O., Engel, A. , Wex, H. & Herrmann, H. (2022). High number concentrations of transparent exopolymer particles in ambient aerosol particles and cloud water - a case study at the tropical Atlantic Ocean. *Atmospheric Chemistry and Physics*, 22 (8). pp. 5725-5742. DOI 10.5194/acp-22-5725-2022.

Poulain, S., & Bourouiba, L. (2018). Biosurfactants Change the Thinning of Contaminated Bubbles at Bacteria-Laden Water Interfaces. *Physical Review Letters*, *121*(20), 204502. https://doi.org/10.1103/PhysRevLett.121.204502

Rastelli, E., Corinaldesi, C., Dell'anno, A., Lo Martire, M., Greco, S., Cristina Facchini, M., Rinaldi, M., O'Dowd, C., Ceburnis, D., & Danovaro, R. (2017). Transfer of labile organic matter and microbes from the ocean surface to the marine aerosol: An experimental approach. *Scientific Reports*, *7*(1), 1–10. https://doi.org/10.1038/s41598-017-10563-z

Reintjes, G., Arnosti, C., Fuchs, B., & Amann, R. (2019). Selfish, sharing and scavenging bacteria in the Atlantic Ocean: a biogeographical study of bacterial substrate utilisation. *ISME Journal*, *13*(5), 1119–1132. https://doi.org/10.1038/s41396-018-0326-3

Robinson, T. B., Wurl, O., Bahlmann, E., Jürgens, K., & Stolle, C. (2019). Rising bubbles enhance the gelatinous nature of the air–sea interface. *Limnology and Oceanography*, *64*(6), 2358–2372. https://doi.org/10.1002/lno.11188

Russell, L. M., Hawkins, L. N., Frossard, A. A., Quinn, P. K., & Bates, T. S. (2010). Carbohydrate-like composition of submicron atmospheric particles and their production from ocean bubble bursting. *Proceedings of the National Academy of Sciences of the United States of America*, *107*(15), 6652–6657. https://doi.org/10.1073/pnas.0908905107

Saint-Macary, A. D., Marriner, A., Barthelmeß, T., Deppeler, S., Safi, K., Santana, R. C., Harvey, M., & Law, C. S. (2023). DMS cycling in the Sea Surface Microlayer in the South West Pacific: 1. Enrichment potential determined using a novel sampler. *Ocean Science*, *19*(1), 1–15. https://doi.org/10.5194/egusphere-2022-499

Sander, R., Keene, W. C., Pszenny, A. A. P., Arimoto, R., Ayers, G. P., Baboukas, E., Cainey, J. M., Crutzen, P. J., Duce, R. A., Hönninger, G., Huebert, B. J., Maenhaut, W., Mihalopoulos, N., Turekian, V. C., & Van Dingenen, R. (2003). Inorganic bromine in the marine boundary layer: A critical review. *Atmospheric Chemistry and Physics*, *3*(5), 1301–1336. https://doi.org/10.5194/acp-3-1301-2003

Sellegri, K., Barthelmeß, T., Trueblood, J., Cristi, A., Freney, E., Rose, C., Barr, N., Harvey, M., Safi, K., Deppeler, S., Thompson, K., Dillon, W., Engel, A., & Law, C. (2023). Quantified effect of seawater biogeochemistry on the temperature

https://doi.org/10.5194/egusphere-2026-1873
Preprint. Discussion started: 10 April 2026

dependence of sea spray aerosol fluxes. *Atmospheric Chemistry and Physics*, *23*(20), 12949–12964. https://doi.org/10.5194/acp-23-12949-2023

Sellegri, K., Harvey, M., Peltola, M., Saint-Macary, A., Barthelmeß, T., Rocco, M., Moore, K. A., Cristi, A., Peyrin, F., Barr, N., Labonnote, L., Marriner, A., McGregor, J., Safi, K., Deppeler, S., Archer, S., Dunne, E., Harnwell, J., Delanoe, J., … Law, C. S. (2023). Sea2Cloud: from biogenic emission fluxes to cloud properties in the South West Pacific. *Bulletin of the American Meteorological Society*, 1017–1043. https://doi.org/10.1175/bams-d-21-0063.1.

Seymour, J. R., Amin, S. A., Raina, J. B., & Stocker, R. (2017). Zooming in on the phycosphere: The ecological interface for phytoplankton-bacteria relationships. *Nature Microbiology*, *2*(January 2018). https://doi.org/10.1038/nmicrobiol.2017.65

Silva, A., Nikzad, S., Barthelmeß, T., Engel., A., Herrmann, H., van Pinxteren, M., Wirtz, K., Wurl, O., and Schartau, M. (2025). Meta-analytical insights into organic matter enrichment in the surface microlayer. *EGUsphere [preprint],* https://doi.org/10.5194/egusphere-2025-4050.

Song, W., Zhao, C., Mu, S., Pan, X., Zhang, D., Al-Misned, F. A., & Mortuza, M. G. (2015). Effects of irradiation and pH on fluorescence properties and flocculation of extracellular polymeric substances from the cyanobacterium Chroococcus minutus. *Colloids and Surfaces B: Biointerfaces*, *128*, 115–118. https://doi.org/10.1016/j.colsurfb.2015.02.017

Sperling, M., Piontek, J., Engel, A., Wiltshire, K. H., Niggemann, J., Gerdts, G., & Wichels, A. (2017). Combined carbohydrates support rich communities of particle-associated marine bacterioplankton. *Frontiers in Microbiology*, *8*(JAN), 1–14. https://doi.org/10.3389/fmicb.2017.00065

Sun, C. C., Sperling, M., & Engel, A. (2018). Effect of wind speed on the size distribution of gel particles in the sea surface microlayer: Insights from a wind-wave channel experiment. *Biogeosciences*, *15*(11), 3577–3589. https://doi.org/10.5194/bg-15-3577-2018

Sun, L., Xu, C., Zhang, S., Lin, P., Schwehr, K. A., Quigg, A., Chiu, M. H., Chin, W. C., & Santschi, P. H. (2017). Light-induced aggregation of microbial exopolymeric substances. *Chemosphere*, *181*, 675–681. https://doi.org/10.1016/j.chemosphere.2017.04.099

Thornton, D. C. O. (2014). Dissolved organic matter (DOM) release by phytoplankton in the contemporary and future ocean. *European Journal of Phycology*, *49*(1), 20–46. https://doi.org/10.1080/09670262.2013.875596

Thornton, D. C. O., Brooks, S. D., & Chen, J. (2016). Protein and carbohydrate exopolymer particles in the sea surface microlayer (SML). *Frontiers in Marine Science*, *3*(AUG), 1–14. https://doi.org/10.3389/fmars.2016.00135

Triesch, N., Van Pinxteren, M., Engel, A., & Herrmann, H. (2021). Concerted measurements of free amino acids at the Cabo Verde islands: High enrichments in submicron sea spray aerosol particles and cloud droplets. *Atmospheric Chemistry and Physics*, *21*(1), 163–181. https://doi.org/10.5194/acp-21-163-2021

Van Pinxteren, M., Robinson, T. B., Zeppenfeld, S., Gong, X., Bahlmann, E., Fomba, K. W., Triesch, N., Stratmann, F., Wurl, O., Engel, A., Wex, H., & Herrmann, H. (2022). High number concentrations of transparent exopolymer particles in ambient aerosol particles and cloud water - A case study at the tropical Atlantic Ocean. *Atmospheric Chemistry and Physics*, *22*(8), 5725–5742. https://doi.org/10.5194/acp-22-5725-2022

https://doi.org/10.5194/egusphere-2026-1873
Preprint. Discussion started: 10 April 2026

Verdugo, P. (2012). Marine microgels. *Annual Review of Marine Science*, *4*, 375–400. https://doi.org/10.1146/annurev-marine-120709-142759

Verdugo, P., Alldredge, A. L., Azam, F., Kirchman, D. L., Passow, U., & Santschi, P. H. (2004). The oceanic gel phase: A bridge in the DOM-POM continuum. *Marine Chemistry*, *92*(1–4), 67–85. https://doi.org/10.1016/j.marchem.2004.06.017

Villermaux, E., Wang, X., & Deike, L. (2022). Bubbles spray aerosols: Certitudes and mysteries. *PNAS Nexus*, *1*(5), 1–13. https://doi.org/10.1093/pnasnexus/pgac261

Wang, W. L., Moore, J. K., Martiny, A. C., & Primeau, F. W. (2019). Convergent estimates of marine nitrogen fixation. *Nature*, *566*(7743), 205–211. https://doi.org/10.1038/s41586-019-0911-2

Wang, X., Deane, G. B., Moore, K. A., Ryder, O. S., Stokes, M. D., Beall, C. M., Collins, D. B., Santander, M. V., Burrows, S. M., Sultana, C. M., & Prather, K. A. (2017). The role of jet and film drops in controlling the mixing state of submicron sea spray aerosol particles. *Proceedings of the National Academy of Sciences of the United States of America*, *114*(27), 6978–6983. https://doi.org/10.1073/pnas.1702420114

Wang, X., Sultana, C. M., Trueblood, J., Hill, T. C. J., Malfatti, F., Lee, C., Laskina, O., Moore, K. A., Beall, C. M., McCluskey, C. S., Cornwell, G. C., Zhou, Y., Cox, J. L., Pendergraft, M. A., Santander, M. V., Bertram, T. H., Cappa, C. D., Azam, F., DeMott, P. J., … Prather, K. A. (2015). Microbial control of sea spray aerosol composition: A tale of two blooms. *ACS Central Science*, *1*(3), 124–131. https://doi.org/10.1021/acscentsci.5b00148

Wilson, T. W., Ladino, L. A., Alpert, P. A., Breckels, M. N., Brooks, I. M., Browse, J., Burrows, S. M., Carslaw, K. S., Huffman, J. A., Judd, C., Kilthau, W. P., Mason, R. H., McFiggans, G., Miller, L. A., Najera, J. J., Polishchuk, E., Rae, S., Schiller, C. L., Si, M., … Murray, B. J. (2015). A marine biogenic source of atmospheric ice-nucleating particles. *Nature*, *525*(7568), 234–238. https://doi.org/10.1038/nature14986

Wobbrock, J. O., Findlater, L., Gergle, D., & Higgins, J. J. (2011). The Aligned Rank Transform for nonparametric factorial analyses using only ANOVA procedures. *Conference on Human Factors in Computing Systems - Proceedings*, 143–146. https://doi.org/10.1145/1978942.1978963

Zamanillo, M., Ortega-Retuerta, E., Nunes, S., Rodríguez-Ros, P., Dall'osto, M., Estrada, M., Sala, M. M., & Simó, R. (2019). Main drivers of transparent exopolymer particle distribution across the surface Atlantic Ocean. *Biogeosciences*, *16*(3), 733–749. https://doi.org/10.5194/bg-16-733-2019

Zhou, J., Mopper, K., & Passow, U. (1998). The role of surface-active carbohydrates in the formation of transparent exopolymer particles by bubble adsorption of seawater. *Limnology and Oceanography*, *43*(8), 1860–1871. https://doi.org/10.4319/lo.1998.43.8.1860